CellPress

Cancer Cell
Article

Drugging MYCN through an Allosteric Transition in Aurora Kinase A

William Clay Gustafson,[1,4,9] Justin Gabriel Meyerowitz,[2,3,4,9] Erin A. Nekritz,[1,4] Justin Chen,[2] Cyril Benes,[7] Elise Charron,[1,2,4] Erin F. Simonds,[2,4] Robert Seeger,[8] Katherine K. Matthay,[1,4] Nicholas T. Hertz,[3] Martin Eilers,[6] Kevan M. Shokat,[3,5] and William A. Weiss[1,2,4,*]

[1]Department of Pediatrics, UCSF Benioff Children's Hospital
[2]Departments of Neurology and Neurological Surgery
[3]Department of Cellular and Molecular Pharmacology
[4]Helen Diller Family Comprehensive Cancer Center
[5]Howard Hughes Medical Institute
University of California, San Francisco, San Francisco, CA 94158, USA
[6]Theodor Boveri Institute, Biocenter, University of Wurzburg, Am Hubland, 97074 Würzburg, Germany
[7]Massachusetts General Hospital Cancer Center, Harvard Medical School, Charlestown, MA 02114, USA
[8]Division of Hematology/Oncology, Children's Hospital Los Angeles, 4650 Sunset Boulevard, Mailstop #57, Los Angeles, CA 90027, USA
[9]Co-first author
*Correspondence: waweiss@gmail.com
http://dx.doi.org/10.1016/j.ccr.2014.07.015

SUMMARY

MYC proteins are major drivers of cancer yet are considered undruggable because their DNA binding domains are composed of two extended alpha helices with no apparent surfaces for small-molecule binding. Proteolytic degradation of MYCN protein is regulated in part by a kinase-independent function of Aurora A. We describe a class of inhibitors that disrupts the native conformation of Aurora A and drives the degradation of MYCN protein across MYCN-driven cancers. Comparison of cocrystal structures with structure-activity relationships across multiple inhibitors and chemotypes, coupled with mechanistic studies and biochemical assays, delineates an Aurora A conformation-specific effect on proteolytic degradation of MYCN, rather than simple nanomolar-level inhibition of Aurora A kinase activity.

INTRODUCTION

MYC proteins are considered undruggable because their DNA-binding domains are composed of two extended alpha helices with no apparent surfaces for small-molecule binding. MYC also regulates as much as a third of the genome, with overexpression proposed to amplify cell-type-specific gene expression rather than modulate a MYC-specific group of genes (Lin et al., 2012; Nie et al., 2012). The transcription of both MYC and MYCN targets may be blocked through bromodomain inhibitors (Delmore et al., 2011; Filippakopoulos et al., 2010; Mertz et al., 2011). Other methods, such as synthetic lethal screens for potential targets, have revealed druggable targets that may act downstream of MYC (Gustafson and Weiss, 2010; Toyoshima et al., 2012). Using an inducible dominant negative MYC protein, others have shown that systemic MYC inhibition is a viable cancer therapeutic strategy (Soucek et al., 2013). However, using current medicinal chemistry, direct and efficient pharmacological targeting of MYC transcription factors has proven challenging, if not impossible (Prochownik and Vogt, 2010).

MYC genes contribute to a wide range of human tumors through overexpression, amplification, translocation, or stabilization of point mutations. The normal concentration of MYC in cells is tightly regulated at the level of protein stability through canonical upstream kinase signaling pathways, including phosphatidylinositol 3-kinase (PI3K)/mammalian target of rapamycin (mTOR), cyclin-dependent kinase 2 (CDK2), and mitogen-activated protein kinase (MAPK). These kinases direct sequential

Significance

MYC genes contribute to a range of cancers, including neuroblastoma and medulloblastoma, where amplification confers a poor prognosis. MYC also regulates as much as a third of the genome, with overexpression proposed to amplify cell-type-specific gene expression. Despite their prominence in cancer, MYC proteins are considered undruggable. We synthesize and characterize a class of conformation-disrupting inhibitors of Aurora A that destabilize interactions between Aurora A and MYCN. These small molecules represent candidate agents to target MYC and MYCN-driven cancers, as well as prototypes for inhibitors that induce an allosteric change to block nonenzymatic functions of kinases.

phosphorylation and dephosphorylation of conserved residues in MYC proteins, which target them for ubiquitination and degradation by the proteasome (reviewed in Gustafson and Weiss, 2010).

The MYC family member MYCN, named based on its association with *MYCN* amplification in the childhood tumor neuroblastoma, is stabilized by Aurora A in a kinase-independent fashion involving protein-protein interaction (Otto et al., 2009). Independent of its effects on MYCN, Aurora A is an attractive cancer target because it regulates entry into mitosis, maturation of centrosomes, cytokinesis, and formation of the bipolar spindle, in part through the phosphorylation of key regulators of proliferation and survival such as p53, BRCA1, and histone H3 (Crosio et al., 2002; Liu et al., 2004; Ouchi et al., 2004; Scrittori et al., 2001; Zhao et al., 2008). Increased Aurora A expression is a negative prognostic factor in neuroblastoma (Shang et al., 2009), and preclinical testing with MLN8237, a specific Aurora A inhibitor, showed significant promise in cell-line xenograft experiments (Maris et al., 2010). Furthermore, the cocrystal structure of MLN8054 (the predecessor of MLN8237) with Aurora A shows a partial shift away from the active state of the kinase, and treatment of MYCN-expressing neuroblastoma with MLN8237 or MLN8054 modestly decreases MYCN (Brockmann et al., 2013; Dodson et al., 2010). This partial effect on MYCN of these compounds may therefore result from the prolonged inhibition of Aurora A kinase activity or a partial shift in the tertiary structure of Aurora A, which subtly weakens the MYCN-Aurora-A complex. Consistent with this modest effect on MYCN, early-phase clinical testing of MLN8237 in patients with *MYCN*-amplified neuroblastoma has shown little efficacy, underscoring the need for inhibitors of Aurora A that more potently block MYCN (Mossé et al., 2012).

RESULTS

Initial Screen for Conformation-Disrupting Aurora A Inhibitors

We hypothesized that the kinase-independent stabilization of MYCN requires a distinct conformation of Aurora A and that we could rationally design specific and potent conformation-disrupting (CD) inhibitors that perturb this protein-protein interaction, effecting the degradation of MYCN. To identify such CD inhibitors we synthesized a set of compounds with either diaminopyrimidine (VX-680-like) or pyrazolopyrimidine (PP-1-like) scaffolds (Figure 1A) predicted to induce a large structural shift in Aurora A. Derivatives of each of these scaffolds were known to bind to Aurora A. Structural data were available on both scaffolds bound to related kinases, and the routes to their synthesis were tractable. To these ATP-competitive cores, we fused biphenyl urea and amide moieties predicted to stabilize distinct conformations of Aurora A (Dietrich et al., 2010; Filomia et al., 2010).

To test whether this panel of 32 putative CD inhibitors would destabilize MYCN, we initially treated Kelly *MYCN*-amplified neuroblastoma cells with these compounds and measured MYCN protein using western blot. We also assessed for the phosphorylation of histone H3 (p-H3), a known substrate for Aurora A and Aurora B and a marker for mitosis. Treatment with several members of the screening panel decreased levels of both MYCN and p-H3 (Figure 1B; Figure S1A available online). In contrast, and as predicted, known inhibitors of Aurora A, VX-680 and MLN8237, blocked histone H3 phosphorylation at 1 μM yet demonstrated very modest effects on the MYCN protein level. Candidate CD inhibitors were subsequently screened against a second *MYCN*-amplified neuroblastoma cell line, SKN-BE(2) (Figure 1C), substantiating CD532 as our most active lead compound.

CD532 Potently Inhibits Aurora A, Causes Loss of MYCN, and Is Cytotoxic in *MYCN*-Amplified Neuroblastoma Cells

To determine the potency of CD532, we first measured its activity using purified Aurora A protein and revealed it as a potent Aurora A kinase inhibitor with an half maximal inhibitory concentration (IC_{50}) of 45 nM (Figures S1B and S1C). CD532 inhibited Aurora A kinase activity in cells as measured by both phosphorylated Aurora A (T288) and p-H3 at short time points to rule out off-target effects (Figure S1D). The treatment of multiple cell lines with CD532, MLN8237, and VX-680 showed dose-dependent loss of MYCN protein with CD532 and little or no response to high concentrations of MLN8237 (Figure 1D; Figures S1E and S1F).

MLN8237 is a relatively selective inhibitor of Aurora A with a IC_{50} of 1.2 nM and 396.5 nM for Aurora A and Aurora B, respectively, whereas VX-680 is potent against both Aurora A and Aurora B, with a IC_{50} of 0.6 nM and 18 nM, respectively (Harrington et al., 2004; Lin et al., 2012; Manfredi et al., 2011; Nie et al., 2012; Otto et al., 2009). Notably, the in vitro (cell-line) activity of CD532 against MYCN paralleled its cell-free in vitro IC_{50} for Aurora A by approximately 10-fold (Figures 1D; Figures S1E and S1F). By contrast, MLN8237 and VX-680 treatment effected little loss of MYCN protein, even at doses 100 to 1,000 times greater than their IC_{50} for Aurora A. MLN8237 and VX-680 upregulated or had little effect on Aurora A protein. CD532, in contrast, downregulated Aurora A protein across cell lines at higher concentrations, consistent with distinct mechanisms of binding underlying these differential effects. At low concentrations of CD532 and short time points, however, the loss of MYCN was apparent, whereas the levels of Aurora A protein were unaffected. These observations are consistent with the degradation of MYCN resulting from CD532 binding rather than from loss of Aurora A protein.

Histone H3 is a known substrate for both Aurora A and Aurora B. Accordingly, the dual inhibition of Aurora A and Aurora B with VX-680 abrogates the phosphorylation of histone H3 at S10. In contrast, MLN8237 caused an initial increase in S10 phosphorylation at lower concentrations, followed by a sharp drop at higher concentrations (Figures 1D; Figures S1E and S1F). This increase in phosphorylation of histone H3 in response to MLN8237 has been described previously and results from Aurora A inhibition with feedback increase in Aurora B activity (Görgün et al., 2010; Wen et al., 2012). CD532 behaves similarly to MLN8237 with regard to histone H3 phosphorylation, consistent with an Aurora-A-selective effect.

We determined the cellular half maximal effective concentration (EC_{50}) at 72 hr against two different *MYCN*-amplified neuroblastoma cell lines, SK-N-BE(2) and Kelly, as 223.2 and 146.7 nM, respectively, for CD532 and as 40.89 and 33.92 nM,

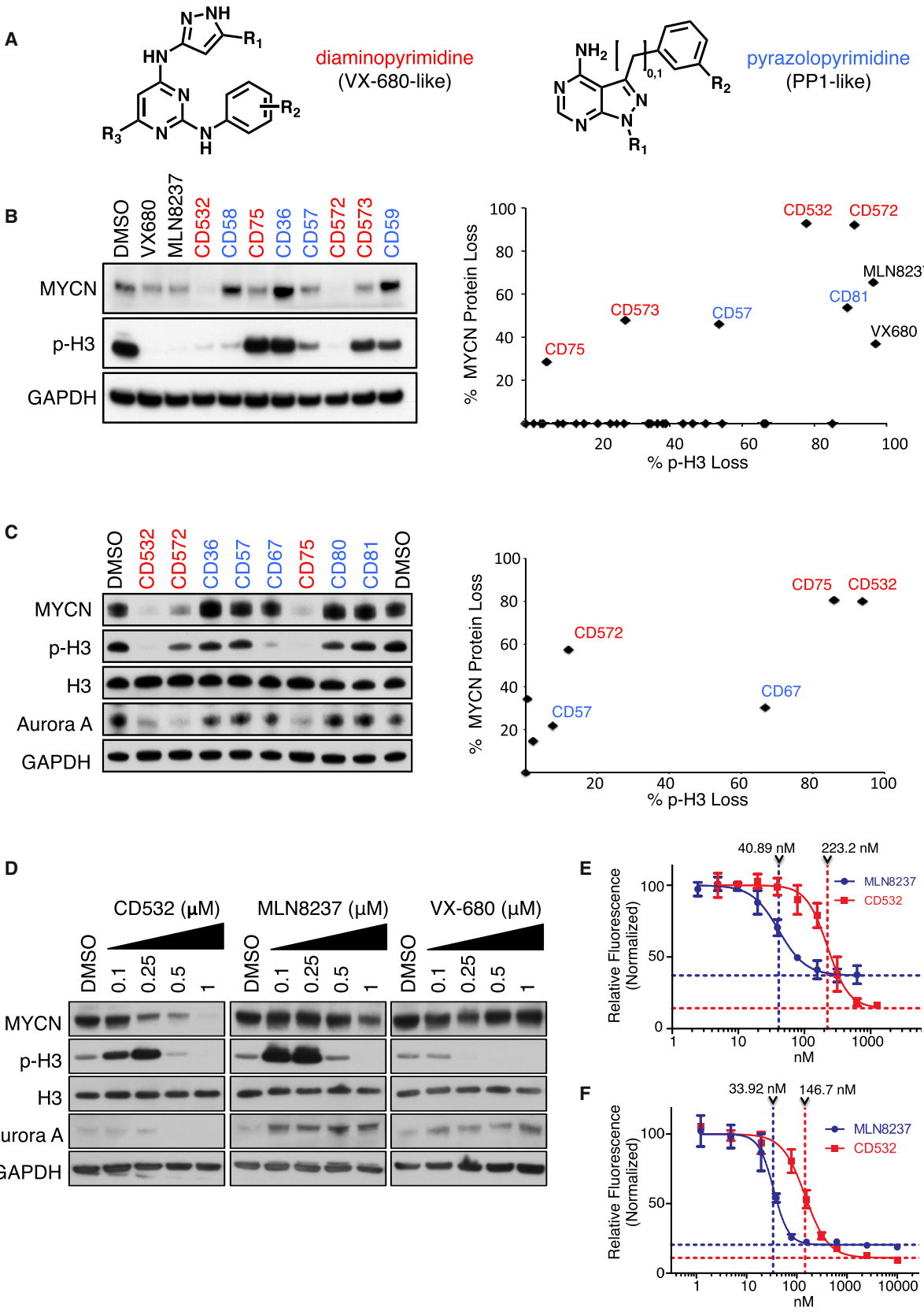

(legend on next page)

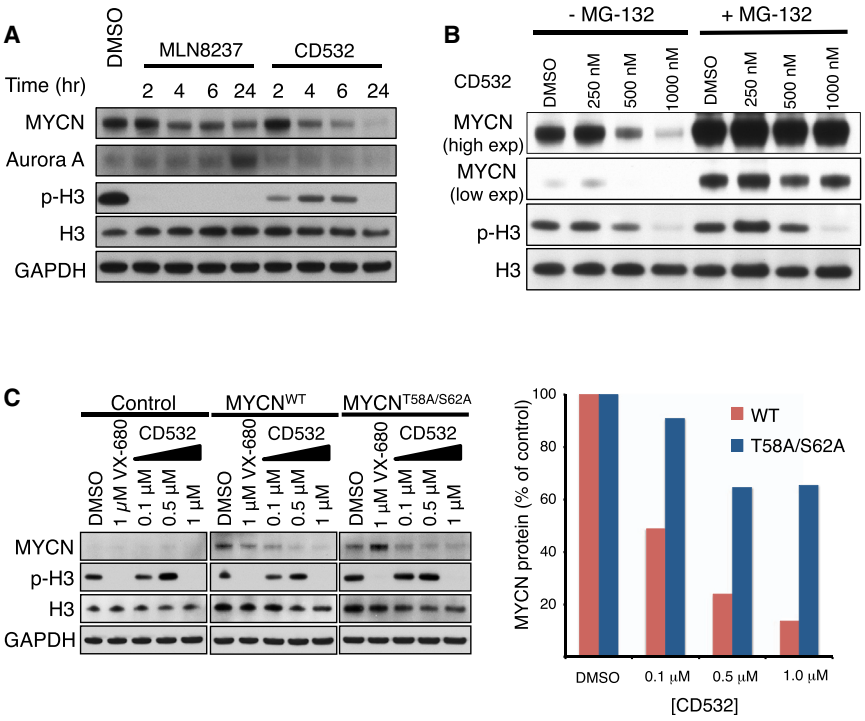

Figure 2. Degradation of MYCN Requires Its Phosphorylation and Is Proteasome Dependent

(A) Immunoblot analysis of the indicated proteins in SK-N-BE(2) cells treated with MLN8237 or CD532 at 1 μM for the indicated durations.

(B) Immunoblot analysis of the indicated proteins in IMR-32 cells treated with the indicated concentrations of CD532 for 2 hr in the absence or presence of MG-132 (4 hr).

(C) Immunoblot analysis of the indicated proteins in the control SHEP cells and SHEP cells ectopically expressing the indicated MYCN treated with the indicated compounds at indicated concentrations for 24 hr.

respectively, for MLN8237 (Figures 1E and 1F). These values are directly proportionate to the cell-free IC_{50} for Aurora A inhibition by CD532 (45 nM) and MLN8237 (4 nM) by ~10 fold. In addition, the IC_{50} of CD532 for on-target MYCN knockdown in SK-N-BE(2) cells (~250 nM; Figure 1D) is consistent with the cellular EC_{50} (223.2 nM; Figure 1E). Notably the maximal cytotoxicity (E_{max}) for each compound is proportionate to the degree of MYCN knockdown rather than the degree of Aurora A inhibition in *MYCN*-amplified neuroblastoma lines. These data argue for an Aurora-A-dependent effect on the inhibition of cell growth and a MYCN-dependent effect on the loss of viability.

Degradation of MYCN Requires Phosphorylation and Proteasomal Degradation of MYCN

Upon the loss of the Aurora A scaffolding function by small interfering RNA (siRNA) knockdown, MYCN is degraded through canonical ubiquitination and proteasomal degradation (Otto et al., 2009). As such, we would expect the rapid degradation of MYCN protein to occur within hours of dissociation of the MYCN-Aurora-A complex. We observed a clear and time-dependent loss of MYCN protein at time points as short as 4 hr of treatment with CD532. In contrast, treatment with MLN8237, although resulting in a similarly rapid decrease in the MYCN level, causes a decrease that is more modest and that does not change over time (Figure 2A). Treatment of MYCN-amplified IMR32 cells with increasing concentrations of CD532 in the presence of the proteasome inhibitor MG-132 shows that MG-132 protects the MYCN from degradation but has no effect on the inhibition of H3 phosphorylation (Figure 2B).

MYCN is sequentially phosphorylated at S62 and T58 before it is ubiquitinated and targeted for degradation. However, when bound in a complex with Aurora A, ubiquitinated MYCN is protected from degradation (Gustafson and Weiss, 2010; Otto et al., 2009). To test whether the activity of CD532 is dependent on these phospho-residues, we treated SHEP *MYCN*-nonamplified neuroblastoma cells engineered to express either wild-type MYCN ($MYCN^{WT}$) or a nonphosphorylatable mutant of MYCN ($MYCN^{T58A/S62A}$) with CD532. CD532 dose-dependently decreased the wild-type MYCN protein but was less effective in degrading $MYCN^{T58A/S62A}$, suggesting that CD532 potentiates the loss of MYCN through the canonical phosphorylation and ubiquitination pathway. Notably, even high concentrations of VX-680, which stabilizes Aurora A in the active conformation (Zhao et al., 2008), had little effect on MYCN protein levels in this system (Figure 2C).

CD532 Stabilizes a DFG-in, Inactive Conformation of Aurora A

CD532 consists of an aminopyrazole-pyrimidine ATP-mimetic backbone, similar to VX-680, but includes a 3-trifluoromethyl-biphenyl urea as its conformation-disrupting pharmacophore

Figure 1. Screening and Characterization of Conformation-Disrupting Aurora A Inhibitor Compounds

(A) The diaminopyrimidine (VX-680-like, red text) and the pyrazolopyrimidine (PP1-like, blue text) scaffolds used for generating the initial screening panel of the compounds. Cell lines were treated for 24 hr with 1 μM of 32 different compounds.

(B and C) Cell extracts of Kelly cells (B) or SK-N-BE(2) cells (C) treated with the indicated compounds at 1 μM for 24 hr were examined using immunoblot as indicated (left); the quantification results (right) are expressed as percentages of the untreated control.

(D) Dose response of SK-N-BE(2) cells to increasing concentrations of CD532, MLN8237, and VX-680.

(E and F) Dose responses of MLN8237 and CD532 at 72 hr using a CyQUANT assay in SK-N-BE(2) (E) and Kelly (F) MYCN-amplified neuroblastoma cells. Error bars represent mean ± SD.

See also Figure S1.

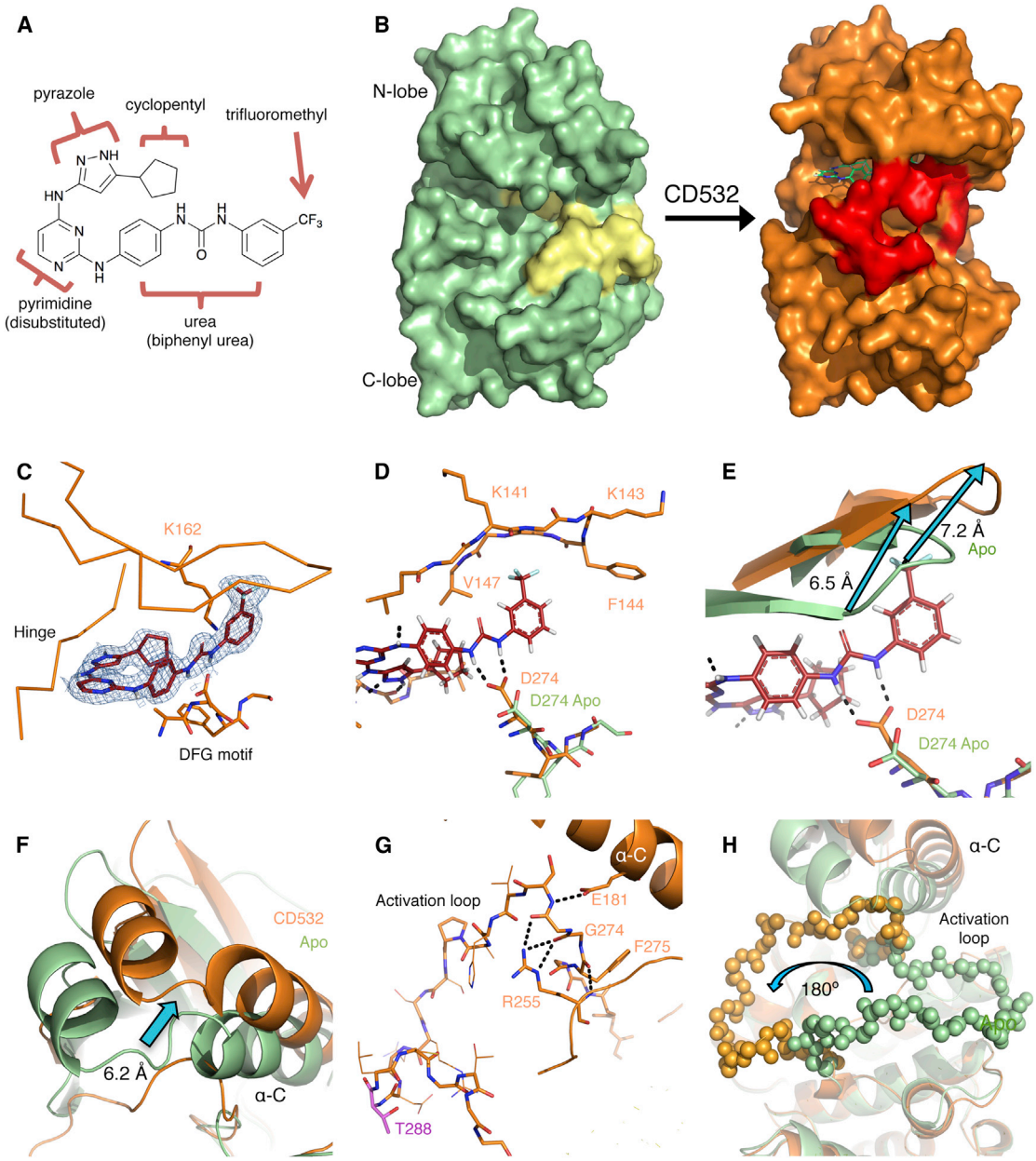

Figure 3. CD532 Stabilizes an Inactive DFG-in Conformation of Aurora A

(A) The structure of CD532 with key components highlighted.
(B) Surface representations of Aurora A apo (green, activation loop in yellow) and of Aurora A bound to CD532 (orange, activation loop in red).
(C) CD532 (red sticks) in ATP binding pocket, overlaid with electron density before ligand fitting (blue mesh).
(D) Interactions among CD532 (red), the DFG motif (D274), and β1/β2 (K141-V147).
(E) Displacement of the glycine-rich loop in the drug-bound structure (orange) compared to apo (green) due to drug binding.
(F and G) Displacement of α-C helix of the N-terminal domain (F) allows for a network of polar contacts among E181, R255, and the DFG motif (G).
(H) Stabilization of the inactive orientation of the activation loop (activation loop in balls). Structural comparisons are all C-terminal alignments.
See also Movie S1 and Table S1.

(Figure 3A). To determine how CD532 binding affects the conformation of Aurora A, we determined the crystal structure of the catalytic domain of Aurora A (residues 123–390) both alone (apo) and bound to CD532, to resolutions of 3.14 and 1.85 Å, respectively (Figure 3B and Table S1). Although the B factor of the relatively disordered activation loop in both structures is high, the tracing of the polypeptide backbone was unambiguous. The electron density for CD532 within the active site was well defined (Figure 3C).

The ATP-binding hinge region of the Aurora A active site makes polar contacts with the aminopyrazole portion of CD532, consistent with our choice of ATP-mimetic scaffold.

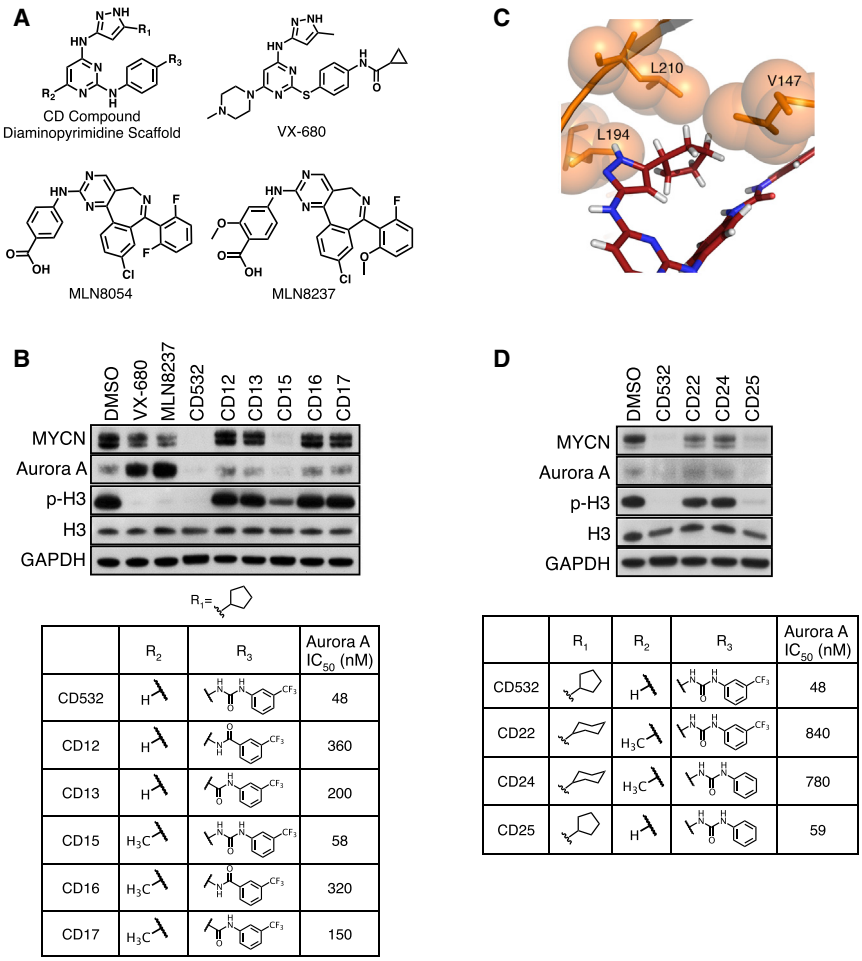

R_1=

	R_2	R_3	Aurora A IC_{50} (nM)
CD532	H		48
CD12	H		360
CD13	H		200
CD15	H_3C		58
CD16	H_3C		320
CD17	H_3C		150

	R_1	R_2	R_3	Aurora A IC_{50} (nM)
CD532		H		48
CD22		H_3C		840
CD24		H_3C		780
CD25		H		59

Figure 4. Structure-Activity Relationships in Inhibiting Aurora A and Reducing MYCN

(A) Chemical structures of CD compound diaminopyrimidine scaffold, VX-680, MLN8054, and MLN8237.

(B) Immunoblot analysis of the indicated proteins in SK-N-BE(2) cells treated with 1 μM of the indicated compound for 24 hr (top) and the structures of CD compounds and their IC_{50} in inhibiting Aurora A kinase activity (bottom).

(C) Hydrophobic packing of cyclopentyl of CD532 among V147, L194, and gatekeeper L210 of Aurora A.

(D) Immunoblot analysis of the indicated proteins in SK-N-BE(2) cells treated with 1 μM of the indicated compound for 24 hr (top) and the structures of CD compounds and their IC_{50} in inhibiting Aurora A kinase activity (bottom).

See also Figure S2.

The catalytic D274 achieves polar contacts with the urea moiety of CD532 to stabilize the biphenyl urea in its orientation toward the N-terminal β1 and β2 strands forming part of the ATP binding pocket (Figures 3C and 3D). The polar contacts between the urea moiety and CD532 allow for an ~7 Å displacement of the β1 and β2 strands in the N-terminal domain via steric clash with the trifluoromethylphenyl moiety of CD532 (Figure 3E). These β1 and β2 strands form part of a β sheet that is the core of the relatively rigid N-terminal domain. Thus displacement of these strands by CD532 disrupts the conformation of Aurora A (apo), rotating and shifting the N-terminal domain by 6.2 Å relative to the C-terminal domain (Figure 3F; Movie S1).

The highly conserved HRD kinase regulatory sequence is located at the lip of the active site. Coordination between this HRD arginine and a phospho-threonine in the activation loop (R255 and T288, respectively, in the case of Aurora A) orients the HRD catalytic aspartic acid to be primed for catalysis. Using this mechanism, the catalytic activity of HRD-containing kinases can be regulated through the phosphorylation of their activation loop. In the presence of CD532, R255 and T288 are displaced by a considerable distance (Figure 3G). In fact, CD532-bound Aurora sequesters R255 in a manner that displaces the catalytic HRD aspartic acid from its catalytically functional orientation, disengaging HRD regulation and stabilizing the kinase in a catalytically inactive conformation.

Indeed, the displaced α-C helix and R255 together trap the most N-terminal portion of the activation loop in a network of hydrogen bonds (Figure 3G). This interaction positions the activation-loop backbone in a manner that stabilizes the entire activation loop in its inactive orientation, flipped 180° relative to its active state (Figure 3H). Thus, CD532 stabilizes Aurora A in a distinct conformation, associated with a 6.2 Å shift in the position of the N-terminal domain relative to the C-terminal domain, a disengaged state of the regulatory HRD motif, and a 180° flip in the activation loop.

Degradation of MYCN Requires Conformation-Specific Inhibition of Aurora A

Although both VX-680 and CD532 bind to the ATP-binding hinge of Aurora A in an identical manner through their aminopyrazole-pyrimidine core, each contains distinct chemical components that produce highly divergent effects on MYCN in cells (Figures 3A and 4A). Our crystallographic data suggest that several chemical moieties of CD532 were critical for its ability to destabilize MYCN. As expected, altering the urea moiety of CD532 decreased the biochemical potency against Aurora A as well as the efficacy against MYCN in neuroblastoma cell lines (Figure 4B). Our structural data also show that the 6 position of the pyrimidine backbone is oriented toward the solvent and the addition of a methyl group to this position (CD15) maintained both cell-free potency and efficacy against MYCN (Figure 4B; Figure S2). These data are consistent with the degradation of MYCN occurring as a consequence of the on-target Aurora A kinase conformation-disrupting activity of CD532.

The cyclopentyl moiety of CD532 packs neatly into a hydrophobic pocket made by V147, L194, and the leucine gatekeeper (L210) (Figure 4C). Thus, our crystallographic data suggest that

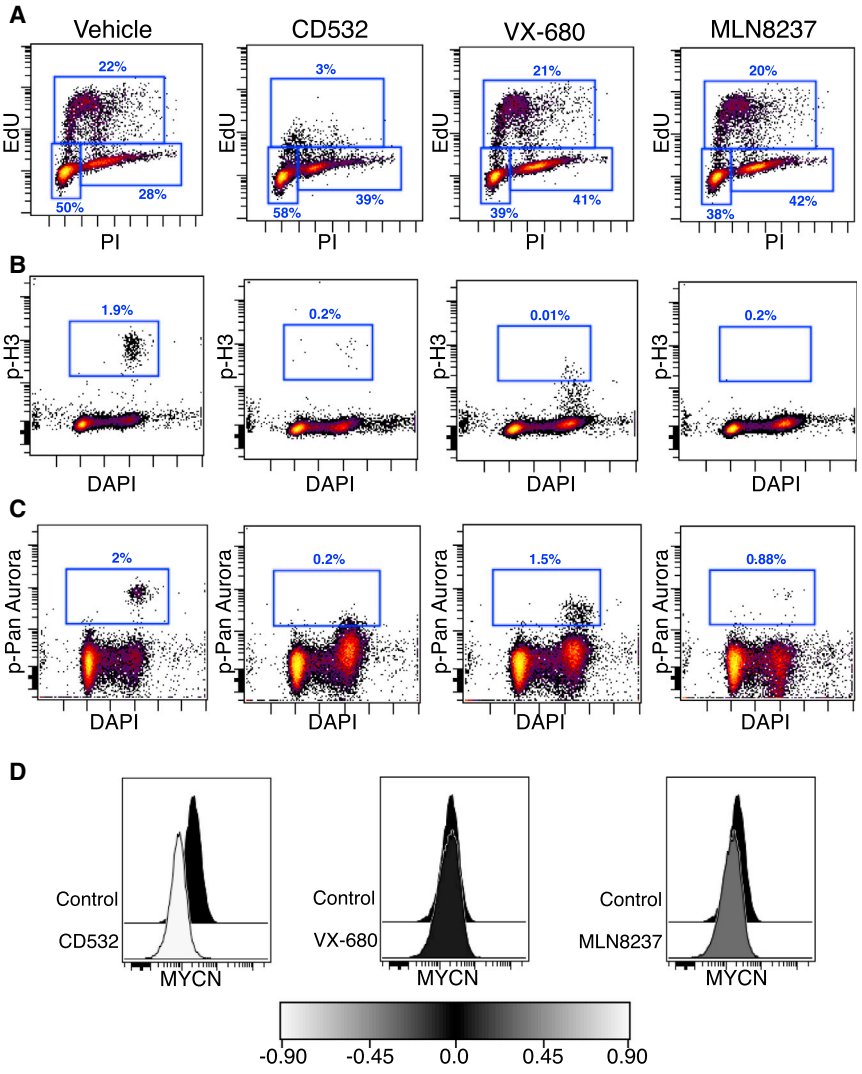

Figure 5. CD532 Inhibits Aurora A Kinase Activity and Downregulates MYCN

SK-N-BE(2) cells were treated for 6 hr with the indicated compounds at 1 μM, and EdU was added 1 hr prior to harvesting to measure the cell cycle using EdU incorporation and propidium iodide (PI) staining (A), using p-H3 (B), using pan-Aurora (A, B, and C isoforms) phosphorylation (C), and using MYCN protein (D) with flow cytometry.

See also Figure S3.

an additional methylene and the adoption of the resulting six-membered ring into a chair conformation would preclude binding to Aurora A without abrogating binding to other kinases with a less bulky gatekeeper. Indeed, compounds CD22 and CD24 lost both potency against Aurora A and efficacy against MYCN (Figure 4D; Figure S2).

The sterically bulky trifluoromethyl interacts with and displaces the β1 and β2 strands, which stabilizes a global conformational change in Aurora A that is unable to protect MYCN from degradation (Figure 3E). We hypothesized that the replacement of this group with a hydrogen would decrease the magnitude of the N-terminal displacement of Aurora A without altering the binding affinity. Indeed, CD25 retained potency against Aurora A activity, demonstrated both biochemically and by the loss of histone H3 phosphorylation, but was less effective than CD532 in driving MYCN loss, suggesting that the magnitude of the N-terminal shift of Aurora A contributes to MYCN destabilization (Figure 4D).

CD532 Blocks S-Phase Entry

Both Aurora A and MYCN are critical to different phases of the cell cycle, and the functional consequences of Aurora A kinase inhibition and MYCN loss are distinct. The inhibition of Aurora A blocks mitosis, causing a G2/M arrest (Manfredi et al., 2011). In contrast, MYC family proteins drive synthesis-phase (S-phase) entry. The knockdown of MYCN protein blocks entry into the S phase, causing a subsequent G0/G1 arrest (Gogolin et al., 2013). To compare the functional differences between conventional Aurora A kinase inhibition (MLN8237 or VX-680) and conformation-disrupting Aurora A kinase inhibition, we treated *MYCN*-amplified neuroblastoma cells and measured cell cycle using flow cytometry. As expected, treatment with MLN8237 or VX-680 resulted in G2/M arrest (Figure 5A; Figure S3), consistent with the inhibition of Aurora A kinase without a significant inhibition of MYCN. By contrast, CD532 resulted in the potent loss of S-phase entry even after 4 or 6 hr of treatment, a result expected in response to the inhibition of MYCN. This loss of S phase was concomitant with the loss of p-H3 (Figures 5A and 5B), the loss of p-pan-Aurora (Figure 5C), and the loss of MYCN protein (Figure 5D). Aurora kinase inhibitors all caused the loss of p-pan-Aurora, detectable in a small fraction of cells using flow cytometry (Figure 5D). All Aurora kinase inhibitors caused the loss of p-pan-Aurora, but only CD532 also caused a loss of S phase and MYCN (Figure 5).

CD532 Is a MYC-Directed Therapy

CD532 has the dual effect of blocking Aurora A kinase activity and driving the degradation of MYCN. To further characterize the effects of CD532 on the cell cycle, we compared it to the bromodomain inhibitor JQ1, which has been shown to block the transcriptional activity of MYCN and the transcription of *MYCN* itself in neuroblastoma (Puissant et al., 2013). The treatment of *MYCN*-amplified neuroblastoma cells with JQ1 for 24 hr resulted in the downregulation of MYCN, blockade of S-phase entry, and accumulation of cells in G0/G1 (Figures 6A; Figures S4A and S4B). The treatment with CD532 for 4 hr resulted in a rapid and potent loss of S phase (consistent with the rapid and potent loss of MYCN protein) and accumulation in both G0/G1 and G2, consistent with a mixed Aurora A and MYCN effect. Treatment with MLN8237 for 4 hr resulted in a modest downregulation of

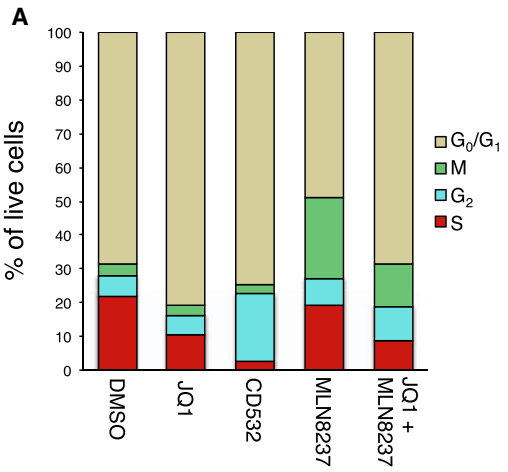

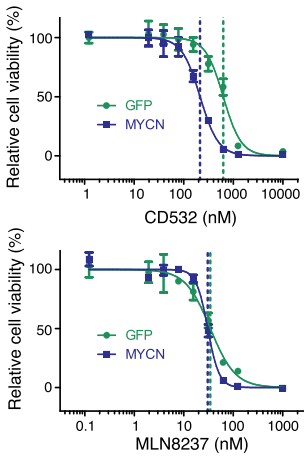

Figure 6. CD532 Acts as a MYCN Inhibitor in Cell Lines

(A) Quantification of the cell cycle of SK-N-BE(2) cells treated with CD532 (1 μM, 4 hr), MLN8237 (0.1 μM, 4 hr), JQ1 (2 μM, 24 hr), and MLN8237 (0.1 μM, 4 hr) in combination with JQ1 (2 μM, 24 hr).

(B) Viability of SHEP cells transduced with MYCN or GFP after 72 hr of treatment with CD532 (top) or MLN8237 (bottom). Error bars represent mean ± SD.

(C) Gene-set-enrichment analysis of 87 cancer cell lines against CD532 dose response showing a positive correlation between MYC genes down and EC_{50} (left) and a negative correlation between MYC genes up and EC_{50} (right).

See also Figure S4 and Table S2.

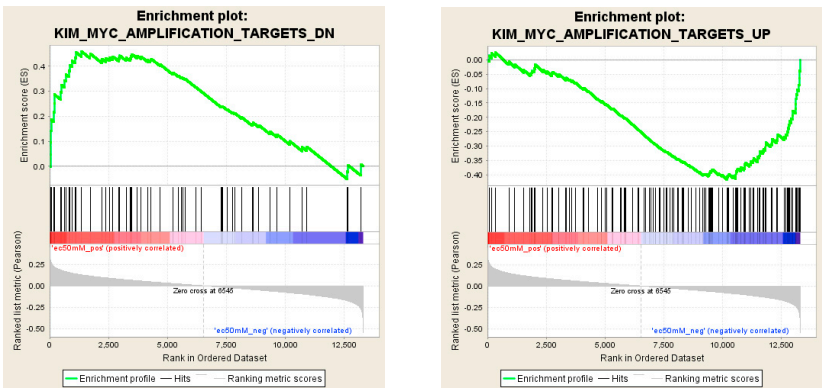

MYCN and accumulation of cells in the G2 and M phase, which has been described previously (Manfredi et al., 2011). When combining treatments with JQ1 for 24 hr and MLN8237 for 4 hr, an additive loss of S phase and accumulation in G2/M were observed, similar to CD532.

That the cell-cycle and viability activity of CD532, but not MLN8237, is related to the degradation of MYCN suggests that the expression of MYCN might confer sensitivity to CD532. We herefore determined the cellular EC_{50} for these compounds against both GFP-and MYCN-transduced SH-EP neuroblastoma cells, which express little to no MYCN. The transduction of MYCN conferred sensitivity to CD532 but not to MLN8237 (Figure 6B). In addition, CD532-driven loss of S phase in these cells could be rescued by the stabilizing $MYCN^{T58A/S26A}$ mutant (Figures S4C and S4D). These data suggest that the efficacy of CD532 is due primarily to the loss of MYCN, whereas that of MLN8237 is due primarily to the inhibition of Aurora A.

To determine whether MYCN might serve as a biomarker of sensitivity to CD532, we screened a panel of 169 distinct tumor-derived and genetically characterized cell lines, including 93 lines for which the information on the *MYCN* copy number was available and 87 lines for which the mRNA expression data were available (Garnett et al., 2012). CD532 showed activity in most cell lines, with the EC_{50} in the nanomolar range, consistent with our results in neuroblastoma (Table S2). Sensitivity to CD532 correlated with the expression of MYCN/MYC mRNA in neuroblastoma cells (Figure S4E). *MYCN*-amplified cell lines were significantly more susceptible to CD532 than were nonamplified lines ($p = 0.0010$). In validation of this analysis, *MYCN* amplified lines were significantly more susceptible to JQ1 than were nonamplified lines ($p = 0.0069$), whereas *MYCN* amplified and nonamplified lines showed similar sensitivities to VX-680 ($p = 0.618$; Figures S4F–S4H). Gene-set-enrichment analysis revealed that susceptibility to CD532 correlated with a MYC signature, i.e., lowest EC_{50} in cells with the highest expression of MYC targets and highest EC_{50} in cells with the downregulated MYC targets (Figure 6C). These data support a broad potential for CD inhibitors of Aurora A against tumors in addition to neuroblastoma and suggest a role for Aurora A CD inhibitors in both MYC- and MYCN-driven diseases.

CD532 Reduces MYCN and Is Effective In Vivo

Although CD532 is a compound in development and not yet optimized for in vivo pharmacokinetics, its efficacy in cell culture was substantial enough to warrant testing in vivo. Studies in mice revealed a serum half-life of ~1.5 hr, providing for an area under the curve during 24 hr (AUC0-24) of 27 μM/hr when delivered at 20 mg/kg (Figure S5A). This is in contrast to the clinically developed MLN8237, which has an AUC0-24 of 78.4 μM/hr when delivered at the same dose (Carol et al., 2011). Nonetheless, treatment of *MYCN*-amplified neuroblastoma xenografts with CD532 led to decreased levels of MYCN protein (Figure 7A; Figure S5B), demonstrating that CD532 can block MYCN protein in vivo.

In addition to neuroblastoma, MYCN prominently drives other cancer types, including medulloblastoma (Swartling et al., 2010). The sonic hedgehog (SHH) subtype of medulloblastoma shows a high expression of MYCN because SHH signaling promotes both the expression and posttranscriptional stabilization of MYCN (Kenney et al., 2003; Thomas et al., 2009). In order to test activity in medulloblastoma in vivo, we treated a MYCN-expressing

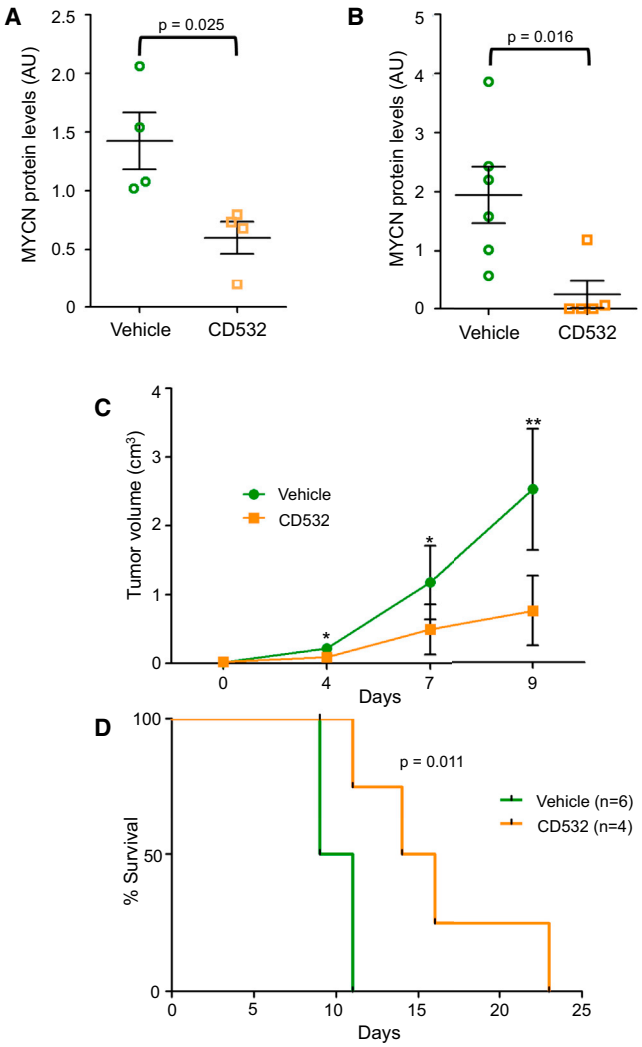

Figure 7. In Vivo Activities of CD532

(A) MYCN protein levels in *MYCN*-amplified SMS-KCN xenografts of tumors from mice treated for 2 days with 60 mg/kg CD532.

(B–D) MYCN protein levels in tumors (B) in, tumor burden (C) of, and survival of (D) mice with subcutaneous SHH-subtype medulloblastoma treated with the vehicle (n = 6) or 25 mg/kg CD532 (n = 4) twice weekly for up to 3 weeks *p < 0.05, **p < 0.005; two-tailed student's t test for (A–C), bars are mean ± SEM; log-rank test for (D), AU, arbitrary units.

See also Figure S5.

SHH-subtype medulloblastoma allograft derived from *Ptch*$^{+/-}$; *p53*$^{-/-}$mice (Kim et al., 2013; Romer et al., 2004). CD532 at 25 mg/kg twice per week substantially reduced MYCN levels, reduced tumor burden, and extended survival in these mice (Figures 7B–7D; Figure S5C). Notably, mice tolerated this dosing regimen without obvious short- or long-term toxicity or weight loss.

Disruption of the MYCN-Aurora-A Complex Depends on the Magnitude of Conformational Change in Aurora A

Despite its potency against Aurora A kinase activity and modest effect on the conformation of Aurora A (Dodson et al., 2010), MLN8237 subtly decreased MYCN protein levels compared to CD532 (Figures 1D and 2A; Figures S1E and S1F). To test how the degree of conformational shift in Aurora A affects the binding of MYCN and Aurora A, we measured the MYCN-Aurora-A interaction in *MYCN*-amplified neuroblastoma cells treated with increasing concentrations of CD532 or MLN8237. CD532 inhibited histone H3 phosphorylation at concentrations 10-fold higher than MLN8237, consistent with their respective biochemical IC_{50} and cellular EC_{50} (Figure 8A). However, CD532 caused a dose-dependent and complete dissociation of the MYCN-Aurora-A complex at 2 hr, whereas MLN8237 only modestly disrupted this interaction (Figures 8A and 8B). This dissociation did not occur with VX-680 treatment (data not shown). The effect of CD532 on the MYCN-Aurora-A interaction was specific in that it did not affect the MYCN-MAX binding (Figures S6A and S6B). Notably, the disruption of the MYCN-Aurora-A complex by CD532 occurred at doses comparable to those required to block p-H3, consistent with the conformation change of MYCN as a consequence of CD532 binding. This is in contrast with MLN8237, which showed only partial disruption of the complex upon maximal Aurora A inhibition (Figure 8A). Thus MLN8237, a more potent Aurora A binder, only modestly decreased the interaction of Aurora A with MYCN. By comparison, CD532 binds Aurora A with lower affinity but has a dramatic effect on Aurora A binding to MYCN (Figure 8B).

As intended through the use of the diaminopyrimidine scaffold for screening, CD532 binds to Aurora A at the hinge region via a pyrazole moiety in a manner similar to VX-680 (Figure 8C) yet interacts with other parts of the Aurora A binding pocket to confer distinct biological effects (loss of MYCN, decreased viability, and loss of S phase), biophysical effects (shift in tertiary structure), and biochemical effects (disruption of the MYCN-Aurora-A complex). The data in Figure 8D demonstrate that VX-680, MLN8237, and CD532 show increasing activity in driving the destabilization of MYCN protein in *MYCN*-amplified cell lines. Comparing the published structures of Aurora A bound to VX-680 and to MLN8054 with our structure of Aurora A bound to CD532 demonstrates a progressive disruption of the conformation of Aurora A (Figure 8E). Thus, the ability of VX-680, MLN8237, and CD532 to progressively displace the α-C helix in Aurora (a structural measure that tracks directly with MYCN proteolysis) illustrates how a starting scaffold can be modified to effect divergent biochemical and biological activities.

DISCUSSION

Earlier studies of Aurora kinases clarified a central role for Aurora A in mitosis and transformation. Inhibitors of Aurora A have therefore been developed as therapeutics and are currently being tested across a range of cancers. Aurora A shares significant structural and sequence similarity with Aurora B, although these proteins have distinct mitotic functions and distinct subcellular localizations. These differences in both function and localization are attributed in part to the association of each kinase with a unique group of cofactor proteins (reviewed in Carmena et al., 2009).

Here we describe a class of compounds that were initially designed to bind Aurora A in a type II fashion, defined by the DFG-out orientation of D274, as a strategy for disrupting the conformation of this kinase. Thus, it was surprising to observe

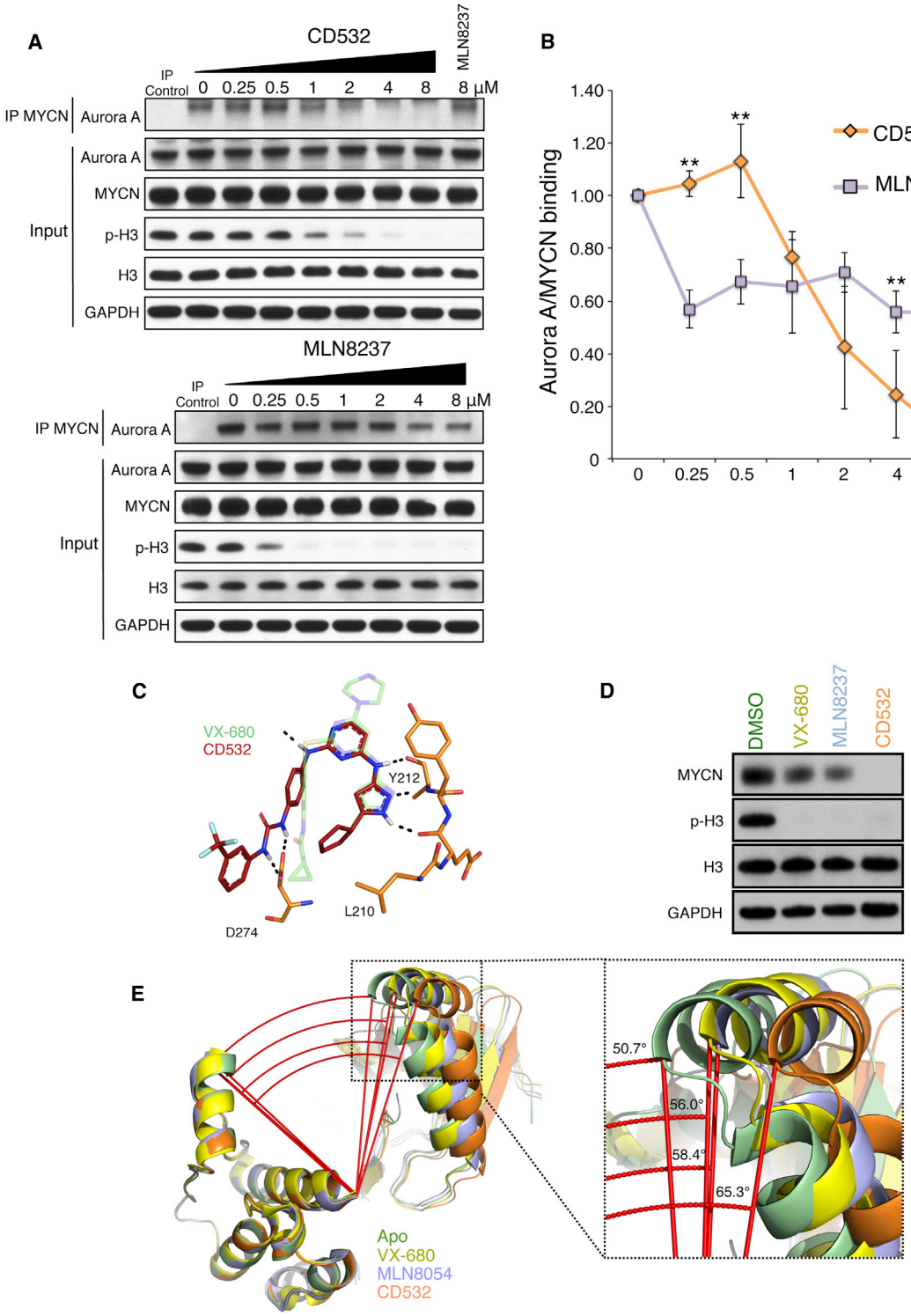

Figure 8. MYCN Loss and Dissociation of the MYCN-Aurora-A Complex Track with the Degree of Conformational Change in Aurora A

(A) Representative immunoblot analysis of immunoprecipitation (IP) of MYCN and total cell lysate (Input) from MYCN-amplified IMR32 cells treated for 4 hr with MG-132 and for 2 hr with increasing concentrations of CD532 or MLN8237.

(B) Quantification of Aurora A and MYCN binding from triplicate experiments (*$p < 0.05$; two-tailed student's t test; bars are mean ± SD).

(C) Comparison of binding modes of VX-680 and CD532.

(D) Immunoblot of MYCN protein after 24 hr treatment of SK-N-BE(2) cells with VX-680, MLN8237, and CD532. See also Figure S6.

(E) Angle between α-Cs of T333, E308, and A172 of Aurora A apo (PDB: 4J8N, green), Aurora A with VX-680 (PDB: 3E5A, yellow), Aurora A with MLN8054 (PDB: 2WTV, purple), and Aurora A with CD532 (PDB: 4J8M, orange).

that CD532 binds Aurora A as DFG-in yet still induces a conformational disruption not achieved by nonselective tool inhibitors that induce a DFG-out conformation in Aurora A in vitro (Martin et al., 2012). Comparing CD532-bound Aurora A to the apo structure shows the activation loop in the inactive orientation, accompanied by a shift in the entire N-terminal domain. Although the activation-loop flip is consistent with an inactive conformation of Aurora A, the urea moiety of CD532 locks the DFG motif in the active DFG-in orientation. This concurrence of features from otherwise distinct states of the kinase is achieved through a steric clash of the trifluoromethylphenyl moiety of CD532 with Aurora's N-terminal β1 and β2 strands, displacing the N-terminal lobe of Aurora A and allowing a unique network of hydrogen bonds to stabilize the activation loop in an inactive orientation.

Our structural data also suggest a mechanism through which an inhibitor can stabilize the inactive conformation of a kinase. Previously described inhibitors that stabilize kinases in their inactive conformation displaced the aspartic acid of the catalytic DFG motif, with a concomitant crankshaft-like 180° rotation of the DFG backbone. In contrast, CD532 induces this inactive conformation through interaction with the β1 and β2 strands of the N-terminal domain, without reorienting the DFG motif. Our structure thus reveals an uncoupling of the DFG flip from the inactive state of a kinase. Whether such uncoupling plays a role in the physiological state of the kinase, perhaps as part of its regulation, or occurs only in the presence of specific pharmacological entities remains to be determined.

Can these specific associations be exploited to identify inhibitors of Aurora kinases that also disrupt interactions with cofactor proteins? The resulting conformation of CD532-bound Aurora A blocks both kinase-dependent and kinase-independent functions of Aurora A. CD532 inhibits Aurora A at low nanomolar concentrations and, in parallel, effects the proteolytic degradation of MYCN. Importantly, we were unable to uncouple kinase inhibition and MYCN proteolysis through the structural modification of CD532, consistent with the disruption of Aurora A's scaffold as a result of bulky pharmacophores that extend from an ATP-competitive core.

The difference in the kinetics of complex dissociation between CD532 and MLN8237, coupled with their respective IC_{50} and crystallographic information, provides insight into the biophysical basis for the disruption of the MYCN-Aurora-A interaction. Although MLN8237 is a potent inhibitor of Aurora A, it only modestly disrupts the conformation of Aurora A. In contrast, CD532 is a weaker inhibitor of Aurora A, but saturating doses lead to the complete dissociation of the complex. Taken together with the structural data, these observations suggest that the equilibrium of dissociation of the MYCN-Aurora-A complex is dependent on the degree of conformational disruption of Aurora A.

Several other inhibitors of Aurora kinase are in clinical development, all of which act as mitotic poisons much like current cytotoxic chemotherapy agents. Our functional data show that CD532 acts more as a potent MYCN inhibitor than as a conventional Aurora A inhibitor in neuroblastoma and has the potential to act as a MYC inhibitor in other cell types. Although the pharmacokinetic properties of CD532 have not been optimized, CD532 could effect the loss of MYCN protein in neuroblastoma xenografts as well as reduce tumor burden and improve survival in a mouse model of medulloblastoma, providing motivation for additional medicinal chemistry and optimization of this family of compounds for clinical use.

Neuroblastoma is the most common extracranial solid tumor of childhood, and *MYCN* amplification is the best-described genetic lesion marking high-risk chemotherapy-resistant disease. The targeted expression of MYCN drives neuroblastoma in mice and zebrafish (Weiss et al., 1997; Zhu et al., 2012). We have previously finessed the destabilization of MYCN through blockade of PI3K/mTOR (Chanthery et al., 2012; Chesler et al., 2006) and have shown in vivo efficacy through an alternative approach to blocking MYCN and its transcriptional targets using BRD4-based bromodomain inhibitors (Puissant et al., 2013). Here we propose a third strategy to block MYCN in cancer. These three interventions, at distinct nodes in the same oncogenic pathway, present a unique opportunity for combinatorial, targeted therapeutics to block emergent resistance while maximizing the blockade of MYCN in neuroblastoma and potentially in other *MYCN*- and *MYC*-driven cancers.

Allostery is most generally defined as a phenomenon whereby a perturbation by an effector at one site of the molecule leads to a functional change at another through the alteration of the shape and/or dynamics (Nussinov and Tsai, 2013). There are several recent examples of allosteric inhibitors for the treatment of cancer, including arsenic trioxide, an antileukemic, that binds to zinc fingers within the PML-RARAα fusion protein of acute promyelocytic leukemia to induce a conformational change favoring oligomerization and eventual degradation (Zhang et al., 2010), and biculutamide, which binds to the androgen receptor to block androgen-receptor-mediated transcription in prostate cancer (Osguthorpe and Hagler, 2011). Enzymes, including but not exclusive to kinases such as Aurora A, may have important nonenzymatic activities, including scaffolding, regulation, and localization of other proteins. As such, many molecular interactions necessary for cellular function and carcinogenesis are not targetable directly with small molecules either because they have no amenable binding pocket (as with MYC proteins) or because their affinity for natural substrate is too high (as with many guanosine triphosphatases [GTPases] such as RAS). By contrast, orthosteric targeting of small molecules to enzymes such as kinases has become relatively trivial. Here we refer to an ATP-mimetic ligand that binds the active site of Aurora A to alter its kinase-independent stabilization of MYCN but also, obligately, its kinase activity. We propose that such an inhibitor be referred to as "amphosteric," denoting an inhibitor that is simultaneously both orthosteric (inhibiting kinase activity) and allosteric (disrupting protein-protein interactions). Thus, CD532 represents the prototype of a class of amphosteric inhibitors that induce an allosteric change to disrupt the nonenzymatic functions of enzymes. Because these amphosteric effects are neglected in most current inhibitor screening, the development of small-molecule screens for other amphosteric inhibitors has the potential to target other undruggable oncoprotein targets.

EXPERIMENTAL PROCEDURES

Cell Culture, Inhibitors, and Western Blotting

Neuroblastoma tumor cell lines were obtained from the University of California San Francisco Cell Culture Facility (Kelly, SK-N-BE2, and SH-EP). SMS-KCN,

SHEP MYCN^{wt} and MYCN$^{T58A/S62A}$ cells were obtained from Martin Eilers lab. All cells were grown in RPMI with 10% fetal bovine serum (FBS). Neuroblastoma cells were harvested and lysed with cell signaling lysis buffer + 1% SDS, sonicated and supernatants boiled in lithium dodecyl sulfate (LDS) sample buffer (Invitrogen). Western blots were performed as described previously (Chanthery et al., 2012), with primary antibodies to MYCN (ab24193, Abcam), histone H3, p-histone H3 (S10), Aurora A (Cell signaling), and glyceraldehyde 3-phosphate dehydrogenase (GAPDH; Millipore). Western blot quantitation was performed using ImageJ software. VX-680 (S1048) and MLN8237 (S1133) were obtained from Selleck chemicals.

Flow Cytometry and Viability

Neuroblastoma cells were treated for the indicated time, trypsinized, washed, stained with Dylight 800 at 0.3 μg/ml (Pierce, 46421), fixed with 1.5% paraformaldehyde (PFA), and permeabilized with 100% methanol. Cells were then stained with antibodies against p-MPM2 (Millipore, 16-155), p-pan-Aurora (Cell Signaling, 2914), MYCN (Thermo, PA5-17403), rabbit immunoglobin G (IgG; Invitrogen, A10542), or mouse IgG (BioLegend, 405307). Cells were stained with DAPI at 0.3 μg/ml (Invitrogen, D21490) and analyzed on the BD LSR II flow cytometer. For cell-cycle analysis, cells were stimulated with EdU for 2 hr prior to harvest and then probed using the Click-iT EdU Flow Cytometry Assay Kit (Invitrogen, C10424). Cells were stained with propidium iodide (BD, 556547) and analyzed on the BD FACSCalibur flow cytometer. The data were gated using Cytobank. For viability studies, neuroblastoma cells were plated in 96-well plates at a density of 1,000 cells/well for SHEP or 4,000 cells/well for Kelly or SK-N-BE2 cells, and then incubated with the indicated concentrations of drug for 72 hr at 37°C. The plates were frozen at −80°C to induce cell lysis. CyQUANT reagent mixture (Invitrogen, C7026) was added to the thawed plates; then the fluorescence was measured. Alternatively, resazurin (Sigma-Aldrich, R7017) was added directly to the wells following the drug treatment; the cells were then incubated for 4 hr at 37°C prior to measuring the fluorescence. The data were analyzed using GraphPad Prism software.

Pulldowns

The cells were pretreated with MG-132 (Calbiochem, 474790) at 5 μg/ml for 4 hr and with a drug (CD532, MLN8237, or VX-680) for 2 hr before lysis with TNN lysis buffer in the presence of a protease inhibitor (Sigma-Aldrich, P8849). Pulldowns were performed with anti-MYCN antibody (Santa Cruz, SC-53993) and Protein G sepharose beads (Sigma-Aldrich, P3296). Immunoblots were performed as previously described.

Chemical Synthesis

Starting materials were purchased from Sigma-Aldrich or Alfa Aesar. Unless otherwise noted, reactions were performed in dry, argon-charged, glass round-bottom flasks and monitored using thin-layer chromatography (TLC) or liquid-chromatography-mass-spectrometry (LC-MS). Compounds were characterized using LC-MS and nuclear magnetic resonance (NMR) spectroscopy. LC-MS retention times (RTs) are reported in minutes based on a gradient of 5%–95% acetonitrile (ACN)/H_2O from $t = 0.1$ min to $t = 1.9$ min. NMR shifts (δ) are reported in parts per million as singlets (s), doublets (d), quartets (q), quintets (quin), or multiplets (m). High-performance liquid chromatography (HPLC) was conducted using a Waters 2545 binary-gradient module, Waters 2767 sample manager, and Waters 2998 photodiode array detector running MassLynx v4.1. Flash/silica gel chromatography was performed on an AnaLogix Intelliflash using SuperFlash Si50 columns (Agilent). Synthetic procedures can be found in the Supplemental Information.

Expression and Purification of Aurora A Kinase

Purification and expression of Aurora A were performed as described previously (Martin et al., 2012), with the following modifications. Aurora A (residues 123–390, T287D) was cloned into a pET28a plasmid providing fusion with a PreScission-Protease-cleavable hexahistidine tag. The protein was overexpressed in BL-21(DE3) cells at 18°C. Digestion with PreScission Protease was performed overnight at 4°C in a 10 kDa molecular-weight-cut-off (MWCO) dialysis cartridge (Thermo Scientific) with a dialysis buffer containing 50 mM 2-(*N*-morpholino)ethanesulfonic acid (MES; pH 6.5), 300 mM NaCl, and 1 mM dithiothreitol (DTT), followed by 4 hr of dialysis with a buffer containing 50 mM MES (pH 6.5) and 1 mM DTT before being loaded onto an ion-exchange column. Pooled fractions were concentrated to 5 mg/ml (Amicon Ultra, 10 kDa MWCO, Millipore) and loaded onto a HiLoad Prep Grade Superdex 200 column (GE Healthcare) equilibrated with 50 mM HEPES (pH 7.4) and 1 mM DTT to yield monomeric enzyme for use in both the kinase assays and crystallization.

In Vivo Studies

For the pharmacokinetic studies, CD532 was formulated at 20 mg/ml in 7.5% DMSO and 92.5% polyethylene glycol 300 (PEG 300). LC-MS/MS detection of CD532 was performed using a Waters 2545 binary-gradient module, Waters 2767 sample manager, and Waters 2998 photodiode array detector running MassLynx v4.1. For the neuroblastoma studies, NOD scid gamma mice (Jackson Laboratory) were implanted with 10^6 SMS-KCN cells in growth media with 50% Geltrex (Invitrogen) into renal capsule. At 21 days post implantation, tumors were palpable and treated for 2 days with 60 mg/kg CD532 before harvesting and flash freezing for analysis. For the medulloblastoma studies, homozygous nu/nu mice (Simonsen) with flank subcutaneous allografts (10^6 cells implanted per mouse) of SHH-subtype MYCN-expressing medulloblastoma were started on treatment once the tumors reached 25 mm^3 in volume (~14 days). Mice were treated with the vehicle (5% DMSO in PEG 300) or CD532 (25 mg/kg, formulated at 7.5 mg/ml) twice per week, delivered by intraperitoneal injection. Mice were euthanized once the maximum tumor length reached 2.0 cm. Difference in tumor burden was evaluated using a two-tailed student's t test, and the difference in survival was evaluated using a log-rank test. All experiments on live vertebrates or higher invertebrates were performed in accordance with relevant institutional and national guidelines and approved by the UCSF Animal Care and Use Committee (IACUC).

Crystallization and Data Collection

After gel separation, the purified fractions of Aurora A were pooled and concentrated in the presence of the drug to a final concentration of 20 mg/ml Aurora A and 1 mM drug. All crystallization reagents were obtained from Hampton Research (Aliso Viejo). Crystals were generated using hanging-drop vapor diffusion at room temperature using a 1:1 mixture of protein solution and well solution. For Aurora A Apo, the well solution consisted of 10% Tacsimate (pH 7.0) and 20% PEG 3,350. For Aurora A with CD532, the well solution consisted of 0.2 M magnesium acetate tetrahydrate, 0.1 M sodium cacodylate trihydrate, and 20% w/v PEG 8,000 (pH 6.0). Crystals did not grow in the apo conditions in the presence of drug or in the drug conditions in the absence of compound. CD532-bound and apo crystals were cryoprotected with well solution supplemented with 10% and 25% ethylene glycol, respectively, and stored in liquid nitrogen. The diffraction data were recorded on Beamline 8.2.2 at the Lawrence-Berkeley Advanced Light Source at a temperature of 100 K and wavelength of 1.0088 nm. The data were indexed using HKL2000 (HKL Research). The drug-bound crystals belong to the C2221 space group with one monomer in the asymmetric unit, and Apo crystals belong to the P31 space group with four monomers in the asymmetric unit. Molecular replacement and refinement were performed using Phaser-MR and phenix.refine in PHENIX (Adams et al., 2010), model building was performed using Coot (Emsley et al., 2010), and figures were drawn using MacPYMOL 1.5.0 (Schrodinger). RCSB validation reports are shown in the Supplemental Information. Procedures for chemical synthesis, gene-set-enrichment analysis, and in vitro kinase assays are described in the Supplemental Information.

ACCESSION NUMBER

Atomic coordinates and structure factors for CD532-bound and apo Aurora A have been deposited in the Protein Data Bank as 4J8M and 4J8N, respectively.

SUPPLEMENTAL INFORMATION

Supplemental Information includes Supplemental Experimental Procedures, six figures, two tables, and one movie and can be found with this article online at http://dx.doi.org/10.1016/j.ccr.2014.07.015.

AUTHOR CONTRIBUTIONS

W.C.G., J.G.M., and E.A.N. designed, performed, and analyzed experiments. E.C. performed and analyzed experiments. J.G.M. and N.T.H. performed chemical synthesis. J.G.M. carried out crystallographic and biochemical studies. J.C. performed bioinformatics analysis. E.F.S. designed and performed flow cytometry experiments. K.K.M., K.M.S., and W.A.W. designed and analyzed experiments. C.B. designed and performed cell line screens. M.E. and R.S. provided reagents. W.C.G., J.G.M., and W.A.W. wrote the manuscript. All authors edited the manuscript. W.C.G. and J.G.M. share equal authorship.

ACKNOWLEDGMENTS

We thank Ulf Peters, Arvin Dar, and Chris Waddling for technical assistance; Yoon-Jae Cho for the medulloblastoma cells; and Alex Warkentin, Mike Lopez, Greg Hamilton, Qi Wen Fan, Miller Huang, Shirin Ilkhanizadeh, and other members of the Shokat and Weiss labs for helpful discussion and critical review. This research was supported by NIH K08NS079485 (W.C.G.); Alex's Lemonade Stand (W.C.G., K.K.M., and W.A.W.); Frank A. Campini Foundation (W.C.G. and K.K.M.); P01CA081403 (W.A.W., K.M.S., K.K.M., and R.S.); F30CA174154 (J.G.M.); CureSearch Grand Challenge Award (W.A.W.); NIH LINCS grant 1U54HG006097-01 (C.B.); R01CA102321 (W.A.W.); R01CA159859 (W.A.W.); R01CA148699 (W.A.W.); P30CA82103 (W.A.W.); Katie Dougherty Foundation (W.A.W. and K.K.M.); Howard Hughes Medical Institute (K.M.S.); and The Samuel Waxman Cancer Research Foundation (K.M.S. and W.A.W.).

Received: February 15, 2013
Revised: May 31, 2014
Accepted: July 17, 2014
Published: August 28, 2014

REFERENCES

Adams, P.D., Afonine, P.V., Bunkóczi, G., Chen, V.B., Davis, I.W., Echols, N., Headd, J.J., Hung, L.-W., Kapral, G.J., Grosse-Kunstleve, R.W., et al. (2010). PHENIX: a comprehensive Python-based system for macromolecular structure solution. Acta Crystallogr. D Biol. Crystallogr. *66*, 213–221.

Brockmann, M., Poon, E., Berry, T., Carstensen, A., Deubzer, H.E., Rycak, L., Jamin, Y., Thway, K., Robinson, S.P., Roels, F., et al. (2013). Small molecule inhibitors of aurora-a induce proteasomal degradation of N-myc in childhood neuroblastoma. Cancer Cell *24*, 75–89.

Carmena, M., Ruchaud, S., and Earnshaw, W.C. (2009). Making the Auroras glow: regulation of Aurora A and B kinase function by interacting proteins. Curr. Opin. Cell Biol. *21*, 796–805.

Carol, H., Boehm, I., Reynolds, C.P., Kang, M.H., Maris, J.M., Morton, C.L., Gorlick, R., Kolb, E.A., Keir, S.T., Wu, J., et al. (2011). Efficacy and pharmacokinetic/pharmacodynamic evaluation of the Aurora kinase A inhibitor MLN8237 against preclinical models of pediatric cancer. Cancer Chemother. Pharmacol. *68*, 1291–1304.

Chanthery, Y.H., Gustafson, W.C., Itsara, M., Persson, A., Hackett, C.S., Grimmer, M., Charron, E., Yakovenko, S., Kim, G., Matthay, K.K., and Weiss, W.A. (2012). Paracrine signaling through MYCN enhances tumor-vascular interactions in neuroblastoma. Sci. Transl. Med. *4*, ra3.

Chesler, L., Schlieve, C., Goldenberg, D.D., Kenney, A., Kim, G., McMillan, A., Matthay, K.K., Rowitch, D., and Weiss, W.A. (2006). Inhibition of phosphatidylinositol 3-kinase destabilizes Mycn protein and blocks malignant progression in neuroblastoma. Cancer Res. *66*, 8139–8146.

Crosio, C., Fimia, G.M., Loury, R., Kimura, M., Okano, Y., Zhou, H., Sen, S., Allis, C.D., and Sassone-Corsi, P. (2002). Mitotic phosphorylation of histone H3: spatio-temporal regulation by mammalian Aurora kinases. Mol. Cell. Biol. *22*, 874–885.

Delmore, J.E., Issa, G.C., Lemieux, M.E., Rahl, P.B., Shi, J., Jacobs, H.M., Kastritis, E., Gilpatrick, T., Paranal, R.M., Qi, J., et al. (2011). BET bromodomain inhibition as a therapeutic strategy to target c-Myc. Cell *146*, 904–917.

Dietrich, J., Hulme, C., and Hurley, L.H. (2010). The design, synthesis, and evaluation of 8 hybrid DFG-out allosteric kinase inhibitors: a structural analysis of the binding interactions of Gleevec, Nexavar, and BIRB-796. Bioorg. Med. Chem. *18*, 5738–5748.

Dodson, C.A., Kosmopoulou, M., Richards, M.W., Atrash, B., Bavetsias, V., Blagg, J., and Bayliss, R. (2010). Crystal structure of an Aurora-A mutant that mimics Aurora-B bound to MLN8054: insights into selectivity and drug design. Biochem. J. *427*, 19–28.

Emsley, P., Lohkamp, B., Scott, W.G., and Cowtan, K. (2010). Features and development of Coot. Acta Crystallogr. D Biol. Crystallogr. *66*, 486–501.

Filippakopoulos, P., Qi, J., Picaud, S., Shen, Y., Smith, W.B., Fedorov, O., Morse, E.M., Keates, T., Hickman, T.T., Felletar, I., et al. (2010). Selective inhibition of BET bromodomains. Nature *468*, 1067–1073.

Filomia, F., De Rienzo, F., and Menziani, M.C. (2010). Insights into MAPK p38alpha DFG flip mechanism by accelerated molecular dynamics. Bioorg. Med. Chem. *18*, 6805–6812.

Garnett, M.J., Edelman, E.J., Heidorn, S.J., Greenman, C.D., Dastur, A., Lau, K.W., Greninger, P., Thompson, I.R., Luo, X., Soares, J., et al. (2012). Systematic identification of genomic markers of drug sensitivity in cancer cells. Nature *483*, 570–575.

Gogolin, S., Ehemann, V., Becker, G., Brueckner, L.M., Dreidax, D., Bannert, S., Nolte, I., Savelyeva, L., Bell, E., and Westermann, F. (2013). CDK4 inhibition restores G(1)-S arrest in MYCN-amplified neuroblastoma cells in the context of doxorubicin-induced DNA damage. Cell Cycle *12*, 1091–1104.

Görgün, G., Calabrese, E., Hideshima, T., Ecsedy, J., Perrone, G., Mani, M., Ikeda, H., Bianchi, G., Hu, Y., Cirstea, D., et al. (2010). A novel Aurora-A kinase inhibitor MLN8237 induces cytotoxicity and cell-cycle arrest in multiple myeloma. Blood *115*, 5202–5213.

Gustafson, W.C., and Weiss, W.A. (2010). Myc proteins as therapeutic targets. Oncogene *29*, 1249–1259.

Harrington, E.A., Bebbington, D., Moore, J., Rasmussen, R.K., Ajose-Adeogun, A.O., Nakayama, T., Graham, J.A., Demur, C., Hercend, T., Diu-Hercend, A., et al. (2004). VX-680, a potent and selective small-molecule inhibitor of the Aurora kinases, suppresses tumor growth in vivo. Nat. Med. *10*, 262–267.

Kenney, A.M., Cole, M.D., and Rowitch, D.H. (2003). Nmyc upregulation by sonic hedgehog signaling promotes proliferation in developing cerebellar granule neuron precursors. Development *130*, 15–28.

Kim, J., Aftab, B.T., Tang, J.Y., Kim, D., Lee, A.H., Rezaee, M., Kim, J., Chen, B., King, E.M., Borodovsky, A., et al. (2013). Itraconazole and arsenic trioxide inhibit Hedgehog pathway activation and tumor growth associated with acquired resistance to smoothened antagonists. Cancer Cell *23*, 23–34.

Lin, C.Y., Lovén, J., Rahl, P.B., Paranal, R.M., Burge, C.B., Bradner, J.E., Lee, T.I., and Young, R.A. (2012). Transcriptional amplification in tumor cells with elevated c-Myc. Cell *151*, 56–67.

Liu, Q., Kaneko, S., Yang, L., Feldman, R.I., Nicosia, S.V., Chen, J., and Cheng, J.Q. (2004). Aurora-A abrogation of p53 DNA binding and transactivation activity by phosphorylation of serine 215. J. Biol. Chem. *279*, 52175–52182.

Manfredi, M.G., Ecsedy, J.A., Chakravarty, A., Silverman, L., Zhang, M., Hoar, K.M., Stroud, S.G., Chen, W., Shinde, V., Huck, J.J., et al. (2011). Characterization of Alisertib (MLN8237), an investigational small-molecule inhibitor of aurora A kinase using novel in vivo pharmacodynamic assays. Clin. Cancer Res. *17*, 7614–7624.

Maris, J.M., Morton, C.L., Gorlick, R., Kolb, E.A., Lock, R., Carol, H., Keir, S.T., Reynolds, C.P., Kang, M.H., Wu, J., et al. (2010). Initial testing of the aurora kinase A inhibitor MLN8237 by the Pediatric Preclinical Testing Program (PPTP). Pediatr. Blood Cancer *55*, 26–34.

Martin, M.P., Zhu, J.-Y., Lawrence, H.R., Pireddu, R., Luo, Y., Alam, R., Ozcan, S., Sebti, S.M., Lawrence, N.J., and Schönbrunn, E. (2012). A novel mechanism by which small molecule inhibitors induce the DFG flip in Aurora A. ACS Chem. Biol. *7*, 698–706.

Mertz, J.A., Conery, A.R., Bryant, B.M., Sandy, P., Balasubramanian, S., Mele, D.A., Bergeron, L., and Sims, R.J. (2011). Targeting MYC dependence in

cancer by inhibiting BET bromodomains. Proc. Natl. Acad. Sci. U.S.A *108*, 16669–16674.

Mossé, Y.P., Lipsitz, E., Fox, E., Teachey, D.T., Maris, J.M., Weigel, B., Adamson, P.C., Ingle, M.A., Ahern, C.H., and Blaney, S.M. (2012). Pediatric phase I trial and pharmacokinetic study of MLN8237, an investigational oral selective small-molecule inhibitor of Aurora kinase A: a Children's Oncology Group Phase I Consortium study. Clin. Cancer Res. *18*, 6058–6064.

Nie, Z., Hu, G., Wei, G., Cui, K., Yamane, A., Resch, W., Wang, R., Green, D.R., Tessarollo, L., Casellas, R., et al. (2012). c-Myc is a universal amplifier of expressed genes in lymphocytes and embryonic stem cells. Cell *151*, 68–79.

Nussinov, R., and Tsai, C.-J. (2013). Allostery in disease and in drug discovery. Cell *153*, 293–305.

Osguthorpe, D.J., and Hagler, A.T. (2011). Mechanism of androgen receptor antagonism by bicalutamide in the treatment of prostate cancer. Biochemistry *50*, 4105–4113.

Otto, T., Horn, S., Brockmann, M., Eilers, U., Schüttrumpf, L., Popov, N., Kenney, A.M., Schulte, J.H., Beijersbergen, R., Christiansen, H., et al. (2009). Stabilization of N-Myc is a critical function of Aurora A in human neuroblastoma. Cancer Cell *15*, 67–78.

Ouchi, M., Fujiuchi, N., Saisal, K., Katayama, H., Minamishima, Y.A., Ongusaha, P.P., Deng, C., Sen, S., Lee, S.W., and Ouchi, T. (2004). BRCA1 phosphorylation by Aurora-A in the regulation of G2 to M transition. J. Biol. Chem. *279*, 19643–19648.

Prochownik, E.V., and Vogt, P.K. (2010). Therapeutic targeting of Myc. Genes Cancer *1*, 650–659.

Puissant, A., Frumm, S.M., Alexe, G., Bassil, C.F., Qi, J., Chanthery, Y.H., Nekritz, E.A., Zeid, R., Gustafson, W.C., Greninger, P., et al. (2013). Targeting MYCN in neuroblastoma by BET bromodomain inhibition. Cancer Discov. *3*, 308–323.

Romer, J.T., Kimura, H., Magdaleno, S., Sasai, K., Fuller, C., Baines, H., Connelly, M., Stewart, C.F., Gould, S., Rubin, L.L., and Curran, T. (2004). Suppression of the Shh pathway using a small molecule inhibitor eliminates medulloblastoma in Ptc1(+/-)p53(-/-) mice. Cancer Cell *6*, 229–240.

Scrittori, L., Hans, F., Angelov, D., Charra, M., Prigent, C., and Dimitrov, S. (2001). pEg2 aurora-A kinase, histone H3 phosphorylation, and chromosome assembly in Xenopus egg extract. J. Biol. Chem. *276*, 30002–30010.

Shang, X., Burlingame, S.M., Okcu, M.F., Ge, N., Russell, H.V., Egler, R.A., David, R.D., Vasudevan, S.A., Yang, J., and Nuchtern, J.G. (2009). Aurora A is a negative prognostic factor and a new therapeutic target in human neuroblastoma. Mol. Cancer Ther. *8*, 2461–2469.

Soucek, L., Whitfield, J.R., Sodir, N.M., Massó-Vallés, D., Serrano, E., Karnezis, A.N., Swigart, L.B., and Evan, G.I. (2013). Inhibition of Myc family proteins eradicates KRas-driven lung cancer in mice. Genes Dev. *27*, 504–513.

Swartling, F.J., Grimmer, M.R., Hackett, C.S., Northcott, P.A., Fan, Q.-W., Goldenberg, D.D., Lau, J., Masic, S., Nguyen, K., Yakovenko, S., et al. (2010). Pleiotropic role for MYCN in medulloblastoma. Genes Dev. *24*, 1059–1072.

Thomas, W.D., Chen, J., Gao, Y.R., Cheung, B., Koach, J., Sekyere, E., Norris, M.D., Haber, M., Ellis, T., Wainwright, B., and Marshall, G.M. (2009). Patched1 deletion increases N-Myc protein stability as a mechanism of medulloblastoma initiation and progression. Oncogene *28*, 1605–1615.

Toyoshima, M., Howie, H.L., Imakura, M., Walsh, R.M., Annis, J.E., Chang, A.N., Frazier, J., Chau, B.N., Loboda, A., Linsley, P.S., et al. (2012). Functional genomics identifies therapeutic targets for MYC-driven cancer. Proc. Natl. Acad. Sci. U.S.A *109*, 9545–9550.

Weiss, W.A., Aldape, K., Mohapatra, G., Feuerstein, B.G., and Bishop, J.M. (1997). Targeted expression of MYCN causes neuroblastoma in transgenic mice. EMBO J. *16*, 2985–2995.

Wen, Q., Goldenson, B., Silver, S.J., Schenone, M., Dancik, V., Huang, Z., Wang, L.-Z., Lewis, T.A., An, W.F., Li, X., et al. (2012). Identification of regulators of polyploidization presents therapeutic targets for treatment of AMKL. Cell *150*, 575–589.

Zhang, X.W., Yan, X.J., Zhou, Z.R., Yang, F.F., Wu, Z.Y., Sun, H.B., Liang, W.X., Song, A.X., Lallemand-Breitenbach, V., Jeanne, M., et al. (2010). Arsenic trioxide controls the fate of the PML-RARalpha oncoprotein by directly binding PML. Science *328*, 240–243.

Zhao, B., Smallwood, A., Yang, J., Koretke, K., Nurse, K., Calamari, A., Kirkpatrick, R.B., and Lai, Z. (2008). Modulation of kinase-inhibitor interactions by auxiliary protein binding: crystallography studies on Aurora A interactions with VX-680 and with TPX2. Protein Sci. *17*, 1791–1797.

Zhu, S., Lee, J.-S., Guo, F., Shin, J., Perez-Atayde, A.R., Kutok, J.L., Rodig, S.J., Neuberg, D.S., Helman, D., Feng, H., et al. (2012). Activated ALK collaborates with MYCN in neuroblastoma pathogenesis. Cancer Cell *21*, 362–373.

Cancer Cell, Volume *26*

Supplemental Information

Drugging MYCN through an Allosteric Transition in Aurora Kinase A

William Clay Gustafson, Justin Gabriel Meyerowitz, Erin A. Nekritz, Justin Chen, Cyril Benes, Elise Charron, Erin F. Simonds, Robert Seeger, Katherine K. Matthay, Nicholas T. Hertz, Martin Eilers, Kevan M. Shokat, and William A. Weiss

Supplemental Data

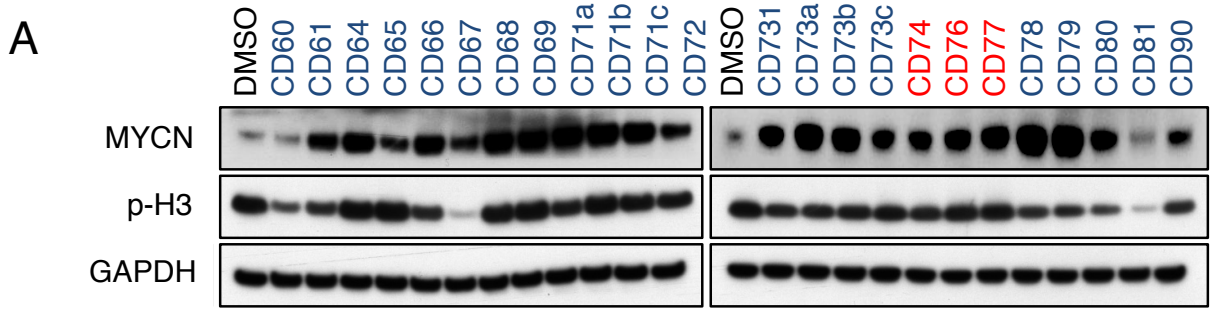

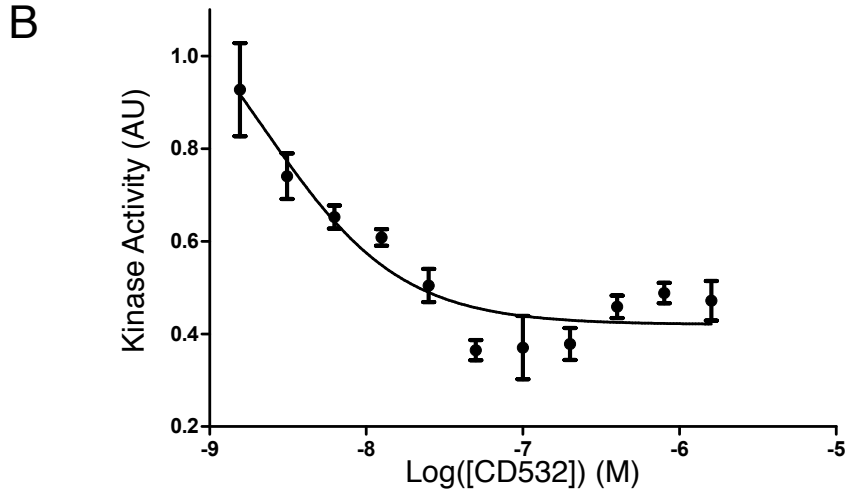

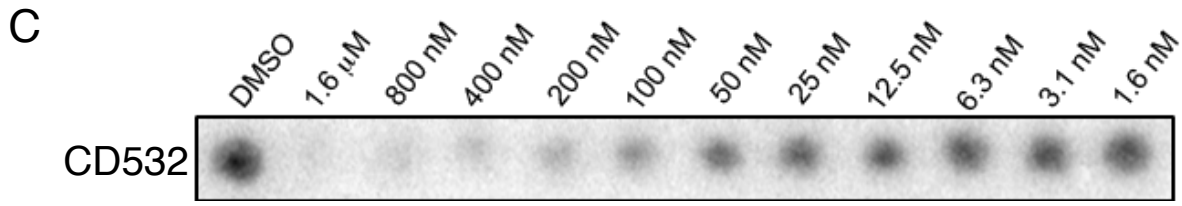

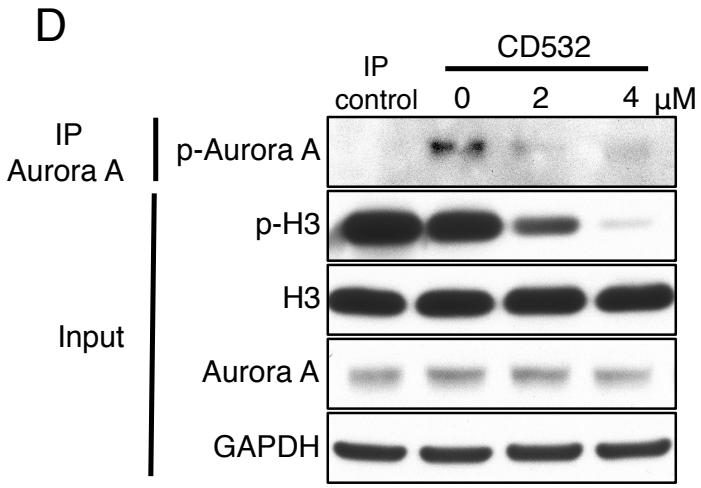

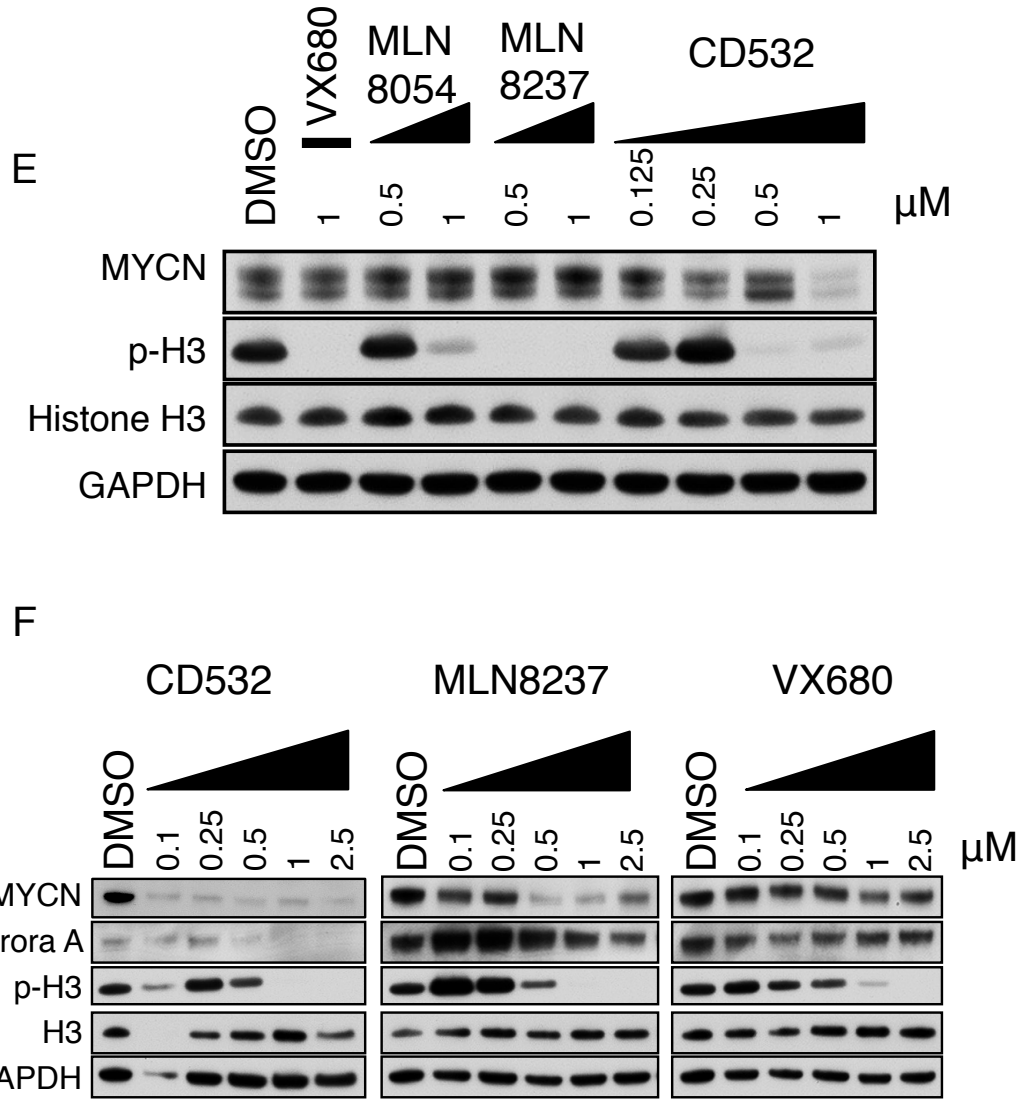

Figure S1, related to Figure 1. Aurora A conformation-disrupting inhibitors induce degradation of MYCN. (A) Screening and characterization of conformation disrupting Aurora A inhibitor (CD) compounds. Screen of Kelly MYCN-amplified cells treated for 24 hr with 1 uM of 32 different compounds predicted to bind to Aurora A and modulate tertiary structure. Extracts examined by western blot for MYCN and phospho-histone H3 expression, quantitation on right (additional blot Figure 1B, quantitation Figure 1B). (B) Representative sigmoidal dose response curve (error bars represent +/- SEM) and (C) 32P ATP blot of CD532 against Aurora A. Enzyme was either full-length or kinase domain-only Aurora A, and substrate was either full-length purified Histone H3 or target oligopeptide. (D) Immunoprecipitation of Aurora A and immunoblot for p-Aurora A (T288) after 2 hr treatment of IMR32 neuroblastoma cells with CD532. Dose response of CD532 in other MYCN amplified neuroblastoma cell lines, (E) SMS-KCN cells or (F) Kelly cells, treated for 24 hr with CD532, MLN8237, MLN8054 or VX-680 and analyzed by immunoblot.

Table S1, related to Figure 3.

	Aurora Kinase A with CD532	**Aurora Kinase A Apo**
Resolution range (Å)	29.07 - 1.853 (1.92 - 1.853)	44.95 - 3.135 (3.247 - 3.135)
Space group	C 2 2 21	P 31
Unit cell	83.175 92.943 74.542 90 90 90	83.783 83.783 171.777 90 90 120
Total reflections		
Unique reflections	24601 (2358)	23663 (2375)
Multiplicity		
Completeness (%)	98.82 (96.05)	99.95 (100.00)
Mean I/sigma(I)	8.53 (2.50)	18.99 (5.50)
Wilson B-factor	28.16	95.57
R-sym		
R-factor	0.1841 (0.2469)	0.1845 (0.2838)
R-free	0.2188 (0.2716)	0.2344 (0.3634)
Number of atoms	4657	17546
macromolecules	2190	8731
ligands	56	
water	172	8
Protein residues	266	1063
RMS(bonds)	0.009	0.004
RMS(angles)	1.19	0.89
Ramachandran favored (%)	97	94
Ramachandran outliers (%)	0	0.95
Clashscore	9.21	13.49
Average B-factor	38	105
macromolecules	37.8	105.1
solvent	40.6	56.4

Summary of data and refinement statistics for crystal structure solutions of Aurora A Apo (4J8N) and Aurora A bound to CD532 (4J8M) generated in PHENIX.

Movie S1, related to Figure 3. Provided as an MPEG file. CD532 stabilizes an inactive conformation of Aurora A. Morph of apo structure of CD532 (4J8N) to CD532-bound structure (4J8M).

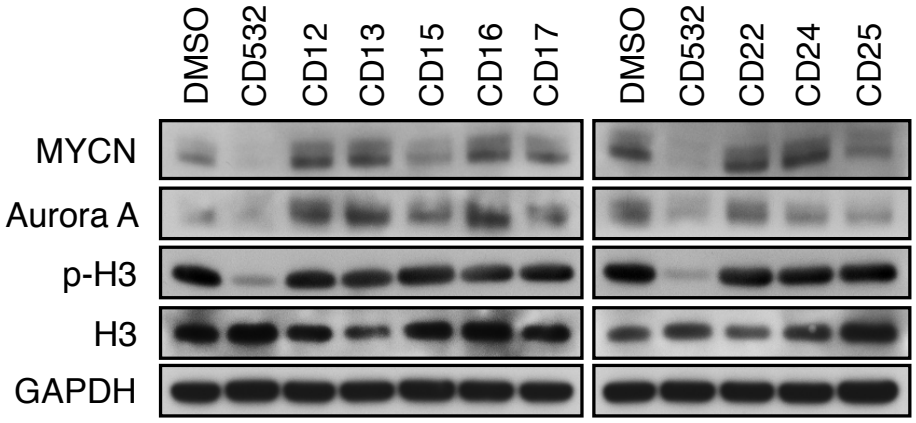

Figure S2, related to Figure 4. Degradation of MYCN requires conformation-specific inhibition of Aurora A. Kelly MYCN amplified neuroblastoma cells were treated with 1 μM of the indicated compounds for 24 hr and a western blot was performed.

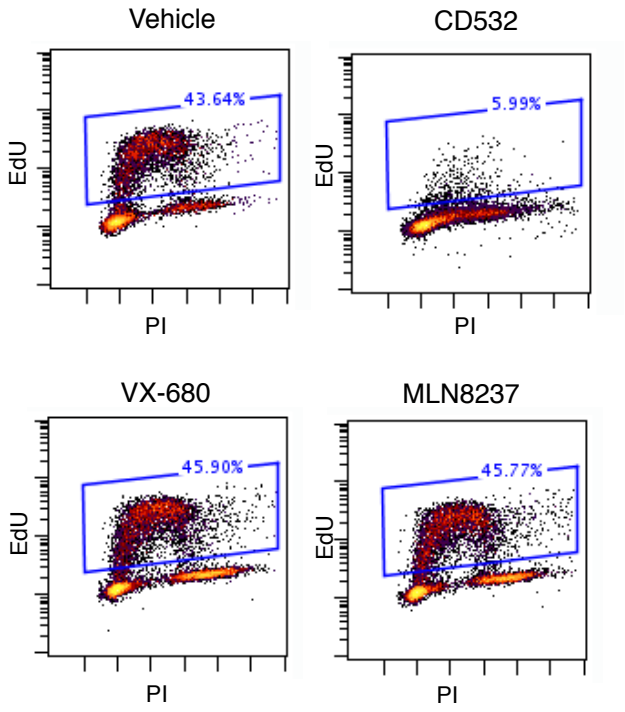

Figure S3, related to Figure 5. CD532 blocks S-phase entry. Cell cycle analysis of MYCN-amplified Kelly neuroblastoma cells treated with 1 μM of the indicated compound for 6 hr.

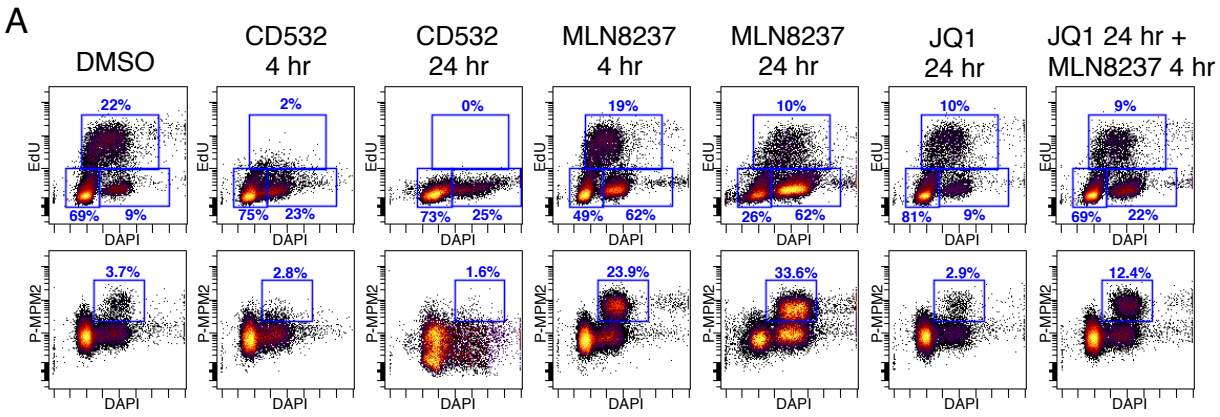
A
DMSO
CD532 4 hr
CD532 24 hr
MLN8237 4 hr
MLN8237 24 hr
JQ1 24 hr
JQ1 24 hr + MLN8237 4 hr
EdU
DAPI
P-MPM2
22%
69%
9%
2%
75%
23%
0%
73%
25%
19%
49%
62%
10%
26%
62%
10%
81%
9%
9%
69%
22%
3.7%
2.8%
1.6%
23.9%
33.6%
2.9%
12.4%

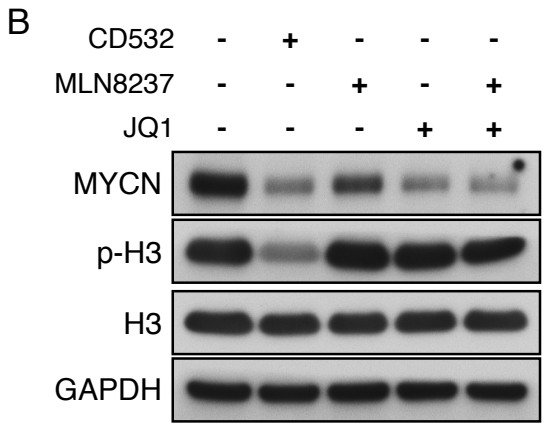
B
CD532
MLN8237
JQ1
MYCN
p-H3
H3
GAPDH

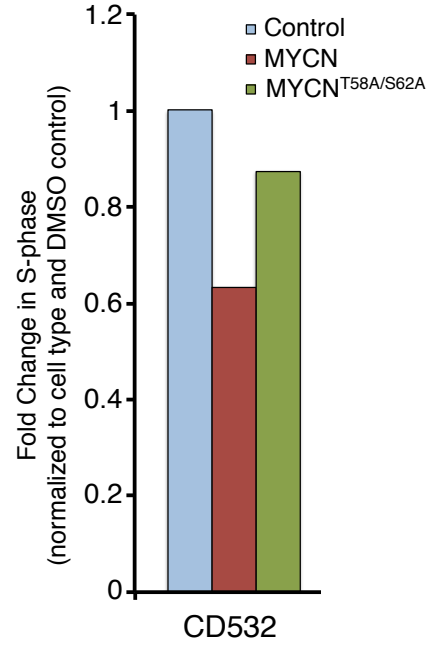
C
Control
MYCN
MYCNT58A/S62A
Fold Change in S-phase
(normalized to cell type and DMSO control)
1.2
1
0.8
0.6
0.4
0.2
0
CD532

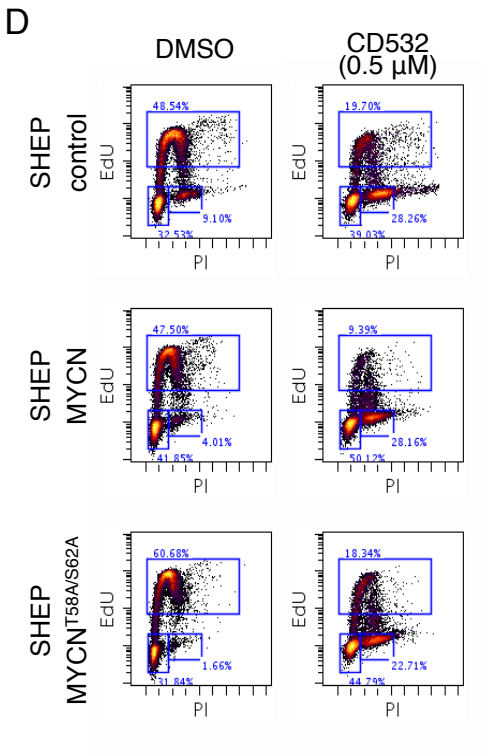
D
DMSO
CD532 (0.5 μM)
SHEP control
SHEP MYCN
SHEP MYCNT58A/S62A
EdU
PI
48.54%
9.10%
19.70%
28.26%
47.50%
4.01%
9.39%
28.16%
60.68%
1.66%
18.34%
22.71%

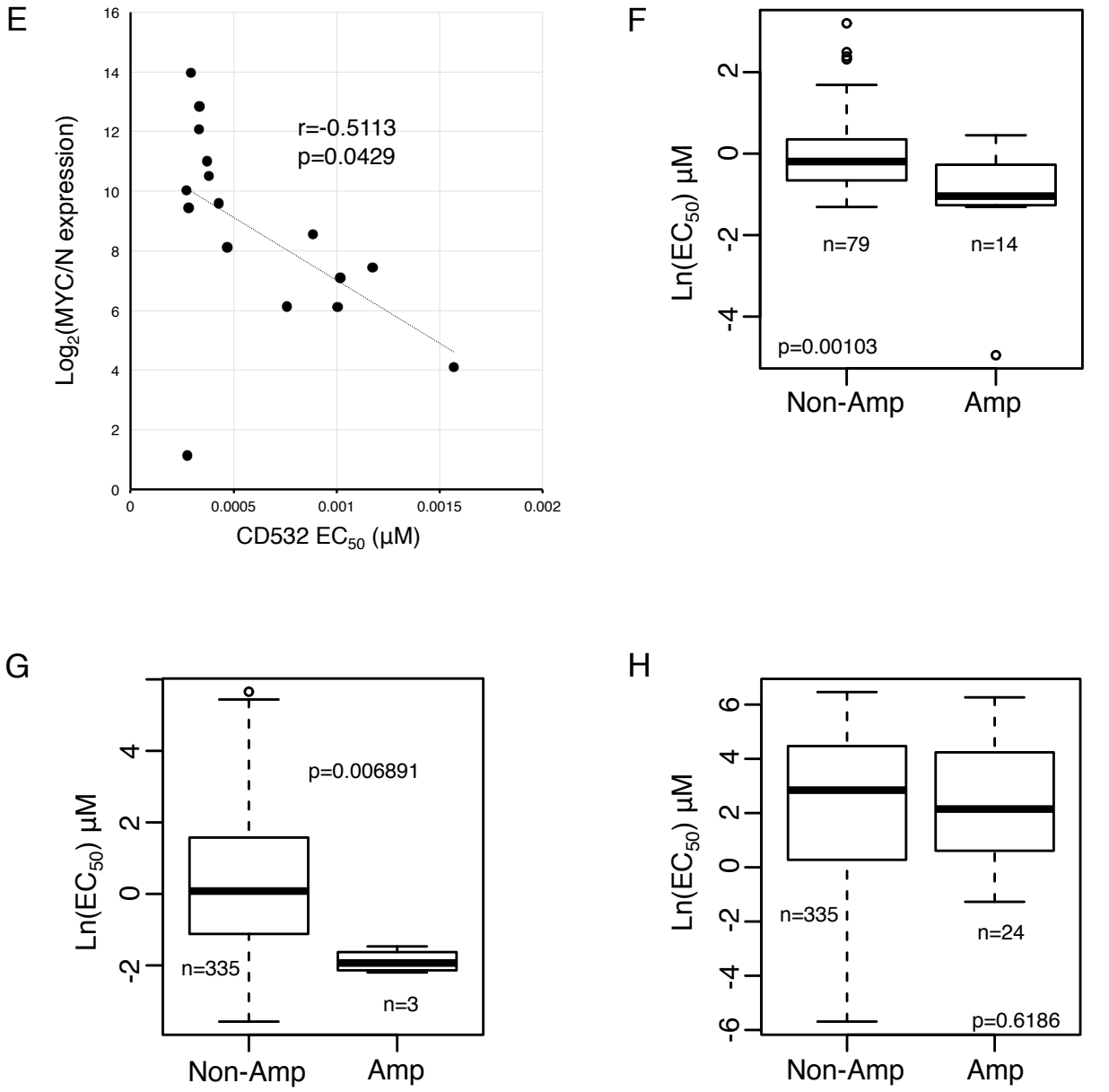

Figure S4, related to Figure 6. CD532 cellular effect is through MYCN inhibition. (A) Scatter plots of EdU staining vs DAPI and pMPM2 staining. Raw data corresponding with cell cycle bar graphs in Figure 6A. (B) Immunoblot demonstrating loss of MYCN in response to treatment with JQ1 and CD532 in SK-N-BE(2) cells corresponding to cell cycle data in Figure S4A and Figure 6A. (C) Quantitation of S-phase fraction and (D) dot plot of SHEP non-MYCN-expressing neuroblastoma transduced with MYCN or mutationally-stabilized $MYCN^{T58A/S62A}$ and treated with MLN8237 or CD532 for 6 hr. (E) Plot of EC50 vs MYC+MYCN mRNA expression. Comparison of EC_{50}s between MYCN amplified vs non-amplified cancer cell lines for (F) CD532 (G) JQ1 and (H) VX-680. Data for MLN8237 or MLN8054 were not available for this analysis. Total n values are from those published and available for JQ1 from Puissant et al. 2014 (G) or for VX680 from the Genomics of Drug Sensitivity in Cancer website (http://www.cancerrxgene.org/downloads).

Table S2, related to Figure 6. Provided as an Excel file. Cancer cell lines profiled through the Genomics of Drug Sensitivity Project with calculated EC_{50}s for CD532.

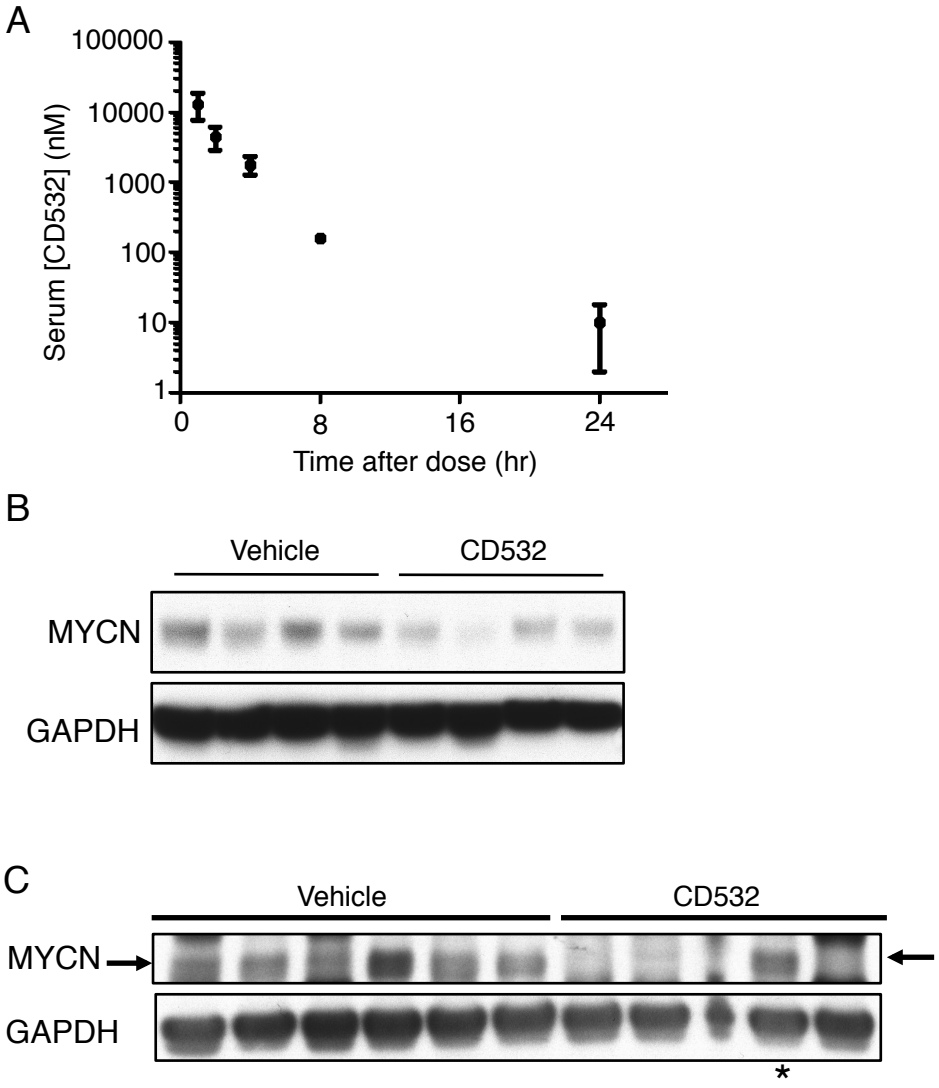

Figure S5, related to Figure 7. CD532 reduced MYCN *in vivo*. (A) Pharmacokinetics of CD532 in mice. CD532 was delivered through intraperitoneal injection at 20 mg/kg and serum levels were measured at 1, 2, 4, 8, and 24 hr. (B) Immunoblot of tumors from mice with MYCN-amplified SMS-KCN xenografts treated for 2 days with 60 mg/kg CD532. (B) Immunoblot of tumors from mice with subcutaneous SHH-subtype medulloblastoma treated with vehicle or 25 mg/kg CD532 twice weekly (error bars +/- SEM).

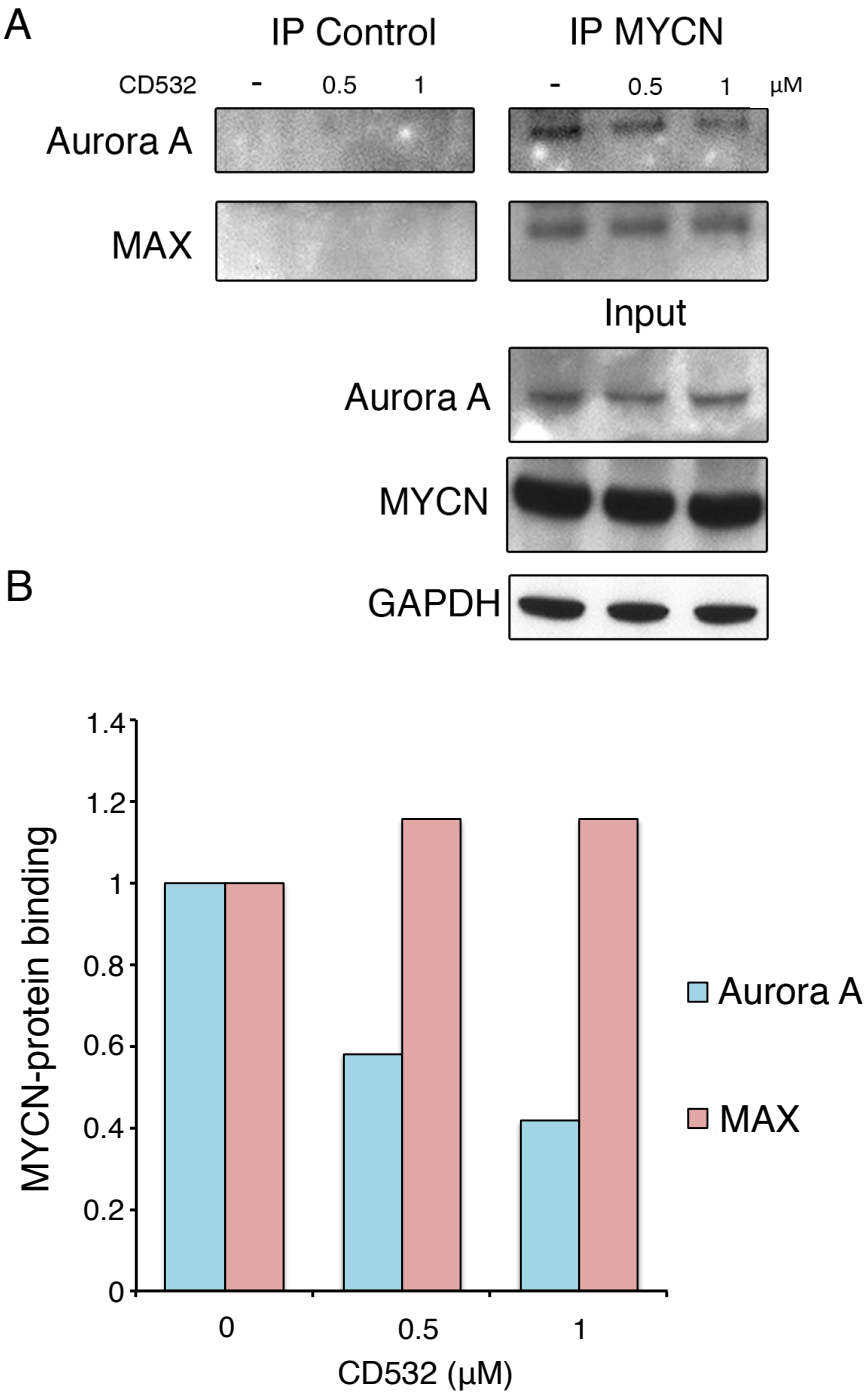

Figure S6, related to Figure 8. CD532 disruption is specific to MYCN-Aurora A complex. (A) SK-N-BE(2) cells were treated with CD532 for 2 hr before immunoprecipitation of MYCN and immunoblot for Aurora A or MAX. (B) Quantitation of MYCN-Aurora A and MYCN-MAX interactions in response to increasing concentration of CD532.

Supplemental Experimental Procedures

Gene Set Enrichment Analysis (GSEA)

Normalized gene expression (Affymetrix HT-HGU133A) was downloaded from the Genomics of Drug Sensitivity in Cancer website (http://www.cancerrxgene.org/downloads/) and log-transformed. 87 cell lines had both unambiguous EC_{50} (calculated using four-parameter non-linear regression within GraphPad Prism) and gene expression data.

GSEA software (Subramanian et al., 2005) was used to identify groups of functionally related genes correlated with sensitivity to CD-532. GSEA was run on these 87 cell lines using the collections of 4,722 curated gene sets (C2) and 615 transcription factor targets (C3) from MSigDB (v4.0). Using the individual EC_{50} of each cell line as a continuous phenotype, genes were ranked using Pearson's correlation, and P values were calculated using 1,000 gene set permutations. Gene sets with less than 15 genes or more than 500 genes were excluded from the analysis. Gene sets with an FDR ≤ 0.05 and a nominal P ≤ 0.05 were considered significant.

Cell-line status for MYCN amplification and drug sensitivity data for VX-680 were downloaded from the Genomics of Drug Sensitivity in Cancer website. Cell-line sensitivity to JQ1 has been previously published (Puissant et al., 2013). Amplified cells possessed MYCN copy number ≥ 8. The significance of sensitivity of CD-532 (EC_{50} calculated using the four-parameter log-logistic function in R using the "drc" package), JQ1, and VX-680 in relation to MYCN amplification status was assessed using the Wilcoxon Rank Sum test in R.

In vitro kinase assays

Kinase assays for Aurora A were performed in 10 mM HEPES pH 7.5, 10 mM $MgCl_2$, 0.01% Triton, 4% v/v DMSO, 5 nM kinase, and either 4 μM histone H3 or 30 μM synthetic peptide AKRRRLSSLRA (Elim Biopharmaceuticals, Inc). Drug concentration ranged from 2000-5 nM. Reactions were preincubated with inhibitor for ten minutes before initiation by addition of 100 μM nonradioactive ATP supplemented with ^{32}P ATP (1 mCi in 200 μL, Perkin-Elmer, 0.8 μCi per reaction). Reactions were quenched at 10 min by spotting 3 μL quantity onto P81 phosphocellulose (Whatman), which were washed 5x5' in 0.1% phophoric acid and dried. Radioactivity was measured by phophorimaging and recorded on a Typhoon fluorescence imager (Molecular Dynamics). Data were quantified using Spot (Knight et al., 2007) and fit to a sigmoidal dose-response curve using Prism software (GraphPad Software, Inc) to obtain IC_{50} values.

Synthetic Procedures

CD532, CD25:

3-cyclopentyl-3-oxopropanenitrile (JM2)

To a dried, argon-charged roundbottom flask with large stir bar was added anhydrous tetrahydrofuran (160 ml), which was then cooled to -78° C before addition of 2.5 M n-Butyllithium in hexanes (64 mL, 160 mmol). Reaction was stirred for 5 minutes before addition of anhydrous acetonitrile (8.48 mL, 160 mmol) dropwise over 5 minutes.

Reaction was stirred for 90 minutes at -78° C, followed by dropwise addition methylcyclopentane carboxylate (10.28 ml, 80.4 mmol) over 10 minutes. Reaction was allowed to stir for another 2 hours at -78o C, allowed to warm to room temperature, and stirred for an additional 30 minutes. Reaction was quenched with 240 ml H2O and stirred until all solids dissolved. Aqueous layer was washed with ether (3x120 ml), and aqueous layer was slowly brought to pH 3.0 with dropwise addition of HCl, forming visible precipitate of product, which was extracted from aqueous with ether (3x120 ml), dried with $MgSO_4$, filtered, and evaporated under reduced pressure to afford 10.4 g (75.9 mmol, 94.4% yield) of a viscous yellow oil. Purity of product was sufficient to carry on to next step. LCMS (RT=1.35): 137.2 (100%); 138.2 (10%); 139.2 (3%).

5-cyclopentyl-1H-pyrazol-3-amine (JM3)

3-cyclopentyl-3-oxopropanenitrile (10.4 g, 75.9 mmol) and hydrazine monohydrate 65% (7.8 ml, 152 mmol) were dissolved in 95% EtOH (85 ml). Reaction was heated to reflux for 2.5 hours and followed to completion by thin layer chromatography. Excess hydrazine and ethanol were evaporated under reduced pressure, crude product dissolved in CHCl3, and purified by flash chromatography with 0-10% MeOH in CHCl3. Recovered 8.93 g (59 mmol, 77.7% yield). LCMS (RT=0.64): 151.3 (100%); 152.4 (14%); 153.4 (4%). NMR, 1H, DMSO (400 MHz): 11.07 (s, 1H), 5.18 (s, 1H), 4.42 (s, 2H), 2.86 (quin, 1H), 1.91-1.48 (m, 8H).

2-chloro-N-(5-cyclopentyl-1H-pyrazol-3-yl)pyrimidin-4-amine (JM5)

5-cyclopentyl-1H-pyrazol-3-amine (1.51 g, 10.0 mmol) and 2,4-dichloropyrimidine (1.49 g, 10 mmol) were dissolved in a 1:1 mixture of THF:H2O (70 ml), and KOAc (98.15 g, 300 mmol) was added to the mixture. Reaction was stirred vigorously at 55° C for 48 hours. Organic layer was separated and evaporated under reduced pressure, dissolved in CH2Cl2 (45 ml), and kept at -20° C for 3 hours. Precipitated solid was filtered, washed with cold CH2Cl2 (15 ml), and dried to yield 0.46 g of N2-(4-aminophenyl)-N4-(5-cyclopentyl-1H-pyrazol-3-yl)pyrimidine-2,4-diamine (1.74 mmol, 17.4% yield). LCMS (RT=1.31): 262.9 (100%); 264.9 (60%); 263.9 (25%); 265.8 (10%). NMR, 1H, DMSO (400 MHz): 12.15 (s, 1H), 10.26 (s, 1H), 8.12 (s, 1H), 2.99 (quin, 1H), 1.98-1.50 (m, 8H).

N2-(4-aminophenyl)-N4-(5-cyclopentyl-1H-pyrazol-3-yl)pyrimidine-2,4-diamine (JM8)

JM5 (78 mg, 0.3 mmol) and p-phenylenediamine (35.6 mg, 0.33 mmol) were dissolved in n-butanol and stirred at 90° C for 3 hr. Solvent was evaporated under reduced pressure and crude product was purified by HPLC (10-75% ACN/H2O) and lyophilized to give 32 mg of JM8 (0.096 mmol, 32% yield). LCMS (RT=0.84): 335.3 (100%); 336.3 (25%); 337.4 (4%). NMR, 1H, DMSO (400 MHz): 9.62 (s, 1H), 8.75 (s, 1H), 8.11 (s, 1H), 7.83 (d, 1H), 7.23 (d, 2H), 6.50 (m, 2H), 6.26 (s, 1H), 6.17 (s, 1H), 2.94 (quin, 1H), 1.94-1.53 (m, 8H).

1-(4-((4-((5-cyclopentyl-1H-pyrazol-3-yl)amino)pyrimidin-2-yl)amino)phenyl)-3-(3-(trifluoromethyl)phenyl)urea (CD532)

JM8 (13.5 mg, 40.3 µmol) was dissolved in DMF (2 ml) in a dry, argon-charged roundbottom flask. 3-(trifluoromethyl)phenyl isocyanate (6.23 µl, 44.3 µmol) was added

and reaction was stirred overnight under argon gas. Crude product was purified by HPLC (10-75% ACN/H2O) and 3.6 mg of NHC53-2 (6.89 µmol, 17% yield) was recovered as a white powder. LCMS (RT=1.32): 522.2 (100%); 523.3 (30%); 524.4 (5%). NMR, 1H, DMSO (400 MHz): 9.69 (s, 1H), 9.51 (s, 1H), 9.29 (s, 1H), 8.94 (s, 1H), 8.25 (s, 1H), 8.04 (s, 1H), 7.91 (d, 1H), 7.65-7.51 (m, 3H), 7.45 (quin, 1H), 7.40-7.32 (m, 2H), 7.23 (d, 1H), 6.32 (s, 1H), 6.19 (s, 1H), 2.93 (quin, 1H), 2.06-1.39 (m, 8H).

3-[4-({4-[(5-cyclopentyl-1H-pyrazol-3-yl)amino]pyrimidin-2-yl}amino)phenyl]-1-phenylurea (CD25)

JM8 (3.0 mg, 8.95 µmol) was dissolved in dry DMF (3 ml) in a dry, argon-charged flask, and isocyanatobenzene (1.07 µl, 9.84 µmol) was added. Reaction was stirred at ambient temperature for 1 hour under positive pressure. Solvent was evaporated under reduced pressure, and product was purified by HPLC (30-70% ACN/H2O) to recover 0.7 mg (17% yield) of a white powder. LCMS (RT=1.22): 454.3 (100%), 455.4 (30%), 456.4 (4%). NMR, 1H, DMSO (400 MHz): 9.51 (s, 1H), 8.94 (s, 1H), 8.68 (s, 1H), 8.58 (s, 1H), 8.14 (s, 1H), 7.92 (s, 1H), 7.57 (d, 2H), 7.42 (m, 2H), 7.32 (d, 2H), 7.24 (d, 2H), 6.91 (s, 1H), 6.33 (s, 1H), 6.18 (s, 1H), 3.70 (s, 1H), 2.96 (s, 1H), 1.98-1.43 (m, 8H).

CD15:

2-chloro-N-(5-cyclopentyl-1H-pyrazol-3-yl)-6-methylpyrimidin-4-amine (JM4)

5-cyclopentyl-1H-pyrazol-3-amine (1.51 g, 10 mmol) and 2,4-dichloro-6-methylpyrimidine (1.63 g, 10 mmol) were dissolved in a 1:1 mixture of THF:H2O (70 ml) and treated with KOAc (29.45 g, 300 mmol). Reaction was stirred vigorously at 55° C for 48 hr. Layers were separated, organic layer was evaporated under reduced pressure, and resulting solid was purified by flash chromatography (2-10% MeOH/CHCl3) to afford 1.69 g (61% yield) of a white powder. LCMS (RT=1.26): 277.2 (100%); 279.2 (60%); 278.3 (25%); 280.2 (8%). NMR, 1H, DMSO (400 MHz): 8.28 (s, 1H), 7.35 (s, 1H), 6.64 (s, 1H), 5.25 (s, 1H), 2.05 (s, 3H), 1.72-1.51 (m, 8H).

N2-(4-aminophenyl)-N4-(5-cyclopentyl-1H-pyrazol-3-yl)-6-methylpyrimidine-2,4-diamine (JM14)

2-chloro-N-(5-cyclopentyl-1H-pyrazol-3-yl)-6-methylpyrimidin-4-amine (73 mg, 0.26 mmol) and p-phenylenediamine (56.2 mg, 0.52 mmol) were dissolved in n-BuOH (3 mL) and stirred at 90° C for 5 hours. Reaction was allowed to cool to ambient temperature, solvent was evaporated under reduced pressure, and product was purified by HPLC (10-75% ACN/H2O) to afford 33 mg (36% yield) of JM14. LCMS (RT=0.84): 349.3 (100%); 350.3 (22%); 351.3 (4%). NMR, 1H, CDCl3: 8.54 (s, 1H), 7.20 (d, 2H), 6.62 (d, 2H), 2.90 (quin, 1H), 2.22 (s, 3H), 1.98-1.93 (m, 2H), 1.75-1.43 (m, 6H).

1-(4-((4-((5-cyclopentyl-1H-pyrazol-3-yl)amino)-6-methylpyrimidin-2-yl)amino)phenyl)-3-(3-(trifluoromethyl)phenyl)urea (CD15)

To a dry, argon-charged roundbottom flask with stir bar was added JM14 (17 mg, 0.049 mmol) and dry DMF. 3-(trifluoromethyl)phenyl isocyanate (13.3 µL, 1.1 eq) was added by syringe and reaction was stirred under argon until depletion of JM14 by LCMS (2 hours). Solvent was evaporated under reduced pressure and solid was

dissolved in minimal DMSO for purification by HPLC (10-90% ACN/H2O) to afford 4.2 mg (16% yield) of a white powder. LCMS (RT=1.33): 536.3 (100%); 537.3 (40%); 538.3 (8%). NMR, 1H, DMSO (400 MHz): 9.39 (s, 1H), 9.28 (s, 1H), 8.93 (s, 1H), 8.89 (s, 1H), 8.17 (s, 1H), 8.03 (s, 1H), 7.61 (d, 2H), 7.54 (d, 1H), 7.44 (t, 1H), 7.32 (d, 2H), 7.24 (d, 1H), 6.28-6.09 (b, 2H), 2.94 (quin, 1H), 2.14 (s, 3H), 2.02-1.88 (m, 2H), 1.77-1.45 (m, 6H).

CD22, CD24:

3-cyclohexyl-3-oxopropanenitrile (JM18)

To a dried, argon-charged roundbottom flask with large stir bar was added anhydrous tetrahydrofuran (80 ml), which was cooled to -78o C before addition of 2.5 M n-Butyllithium in hexanes (32 mL, 80 mmol). Reaction was stirred for 5 minutes before addition of anhydrous acetonitrile (4.23 mL, 80 mmol) dropwise over 5 minutes. Reaction was stirred for 90 minutes at -78o C, followed by dropwise addition of methylcyclohexane carboxylate (5.72 ml, 40 mmol) over 15 minutes. Reaction was allowed to stir for another 2 hours at -78o C, allowed to warm to room temperature, and stirred for an additional 30 minutes. Reaction was quenched with 100 ml H2O and stirred until all solids dissolved. Aqueous layer was washed with ether (2x100 ml), and aqueous layer was slowly brought to pH 3.0 with dropwise addition of HCl, forming visible precipitate of product, which was extracted from aqueous with ether (3x100 ml), dried with MgSO4, filtered, and evaporated under reduced pressure to yield 5.3 g (87.6% yield) of a viscous yellow oil. Purity of product was sufficient to carry on to next step. LCMS (RT=1.36): 151.2 (100%), 152.2 (12%), 153.2 (3%).

5-cyclohexyl-1H-pyrazol-3-amine (JM19)

3-cyclohexyl-3-oxopropanenitrile (5.3 g, 35 mmol) was dissolved in 95% EtOH (45 ml), to which was added hydrazine monohydrate (3.5 ml, 70 mmol). Reaction was stirred under reflux for 2.5 hr, solvent was evaporated under reduced pressure, and product was purified by flash chromatography (0-10% MeOH/CHCl3) to give 3.52 g (61% yield) of a viscous reddish oil. LCMS (RT=0.89): 165.3 (100%), 166.3 (20%), 167.3 (8%). NMR, 1H, DMSO (400 MHz): 10.97 (s, 1H), 5.13 (s, 1H), 4.34 (s, 2H), 2.39 (m, 1H), 1.80-1.15 (m, 10H).

2-chloro-N-(5-cyclohexyl-1H-pyrazol-3-yl)-6-methylpyrimidin-4-amine (JM20)

5-cyclohexyl-1H-pyrazol-3-amine (1.65 g, 10 mmol) and 2,4-dichloro-6-methylpyrimidine (1.63 g, 10 mmol) were dissolved in a 1:1 mixture of THF/H2O (70 ml) in a roundbottom flask with stir bar. Reaction was treated with KOAc (30 eq, 29.45 g) and stirred vigorously for 48 hours at 55º C. Organic layer was separated and evaporated under reduced pressure, and crude product was dissolved in CHCl3 (10 ml) and purified by flash column chromatography (0-10% MeOH/CHCl3) to recover 1.14 g (39% yield) of a white powder. LCMS (RT=1.51): 291.3 (100%), 293.2 (60%), 292.3 (28%), 294.2 (10%). NMR, 1H, DMSO (400 MHz): 9.87 (s, 1H), 9.09 (s, 1H), 6.85 (s, 1H), 6.01 (s, 1H), 2.61 (quin, 1H), 2.27 (s, 3H), 1.79-1.21 (m, 10H).

2-N-(4-aminophenyl)-4-N-(5-cyclohexyl-1H-pyrazol-3-yl)-6-methylpyrimidine-2,4-diamine

(JM21)

JM20 (231 mg, 0.79 mmol) and p-phenylenediamine (94.0 mg, 0.87 mmol) were dissolved in n-butanol (6 ml) and stirred at 85o C for 2.5 hr under argon gas. Solvent was evaporated under reduced pressure, crude solid was dissolved with DMSO (1 ml) and 1:1 ACN/H2O (8 ml) and purified by HPLC (5-25% ACN/H2O) to yield 74 mg (20% yield) of a grey powder. LCMS (RT=0.99): 364.3 (100%), 365.3 (20%), 366.3 (4%). NMR, 1H, CDCl3: 8.41 (s, 1H), 7.18 (d, 2H), 6.60 (d, 2H), 6.04 (s, 1H), 5.97 (s, 1H), 3.95 (s, 2H), 3.76 (m, 3H), 2.22 (s, 3H), 1.94-1.09 (m, 10H).

3-[4-({4-[(5-cyclohexyl-1H-pyrazol-3-yl)amino]-6-methylpyrimidin-2-yl}amino)phenyl]-1-[3-(trifluoromethyl)phenyl]urea (CD22)

JM21 (3.9 mg, 10.7 µmol) was dissolved in DMF (3 ml) in a dry, argon-charged roundbottom flask. 3-(trifluoromethyl)phenyl isocyanate (1.65 µl, 11.8 µmol) was added and reaction was stirred for 4 hours under argon gas. Product was purified by HPLC (20-75% ACN/H2O) and 3.05 mg of a white powder (5.54 µmol, 52% yield) was recovered. LCMS (RT=1.40): 550.3 (100%), 551.4 (30%), 552.4 (4%). NMR, 1H, DMSO (400 MHz): 9.40 (s, 1H), 9.14 (s, 1H), 8.95 (s, 1H), 8.75 (s, 1H), 8.14 (s, 1H), 8.04 (s, 1H), 7.61 (d, 2H), 7.52-7.42 (m, 2H), 7.33 (d, 2H), 7.25 (d, 1H), 6.17 (b, 2H), 2.53 (quin, 1H), 2.14 (s, 3H), 1.94-1.81 (m, 2H), 1.79-1.65 (m, 2H), 1.59-1.55 (m, 1H), 1.37-1.18 (m, 5H).

3-[4-({4-[(5-cyclohexyl-1H-pyrazol-3-yl)amino]-6-methylpyrimidin-2-yl}amino)phenyl]-1-phenylurea (CD24)

JM21 (3.9 mg, 10.7 µmol) was dissolved in DMF (3 ml) in a dry, argon-charged roundbottom flask. Phenyl isocyanate (1.28 µl, 11.8 µmol) was added and reaction was stirred for 4 hours under argon gas. Product was purified by HPLC (30-75% ACN/H2O) and 2.15 mg of a white powder (4.46 µmol, 42% yield) was recovered. LCMS (RT=1.27): 482.3 (100%), 483.3 (28%), 484.3 (7%). NMR, 1H, DMSO (400 MHz): 9.40 (s, 1H), 8.92 (s, 1H), 8.86 (s, 1H), 8.74 (s, 1H), 8.19 (s, 1H), 7.59 (d, 2H), 7.42 (d, 2H), 7.31 (d, 2H), 7.23 (t, 2H), 6.90 (t, 1H), 6.22 (s, 1H), 6.14 (s, 1H), 2.53 (m, 1H), 2.14 (s, 3H), 1.86 (m, 2H), 1.72 (m, 2H), 1.59 (m, 1H), 1.35-1.18 (m, 5H).

CD12, CD13, CD16, CD17:

4-nitro-N-[3-(trifluoromethyl)phenyl]benzamide (JM6)

3-(trifluoromethyl)aniline (7.55 ml, 60 mmol) was dissolved in pyridine (200 ml) at ambient temperature under argon gas. 4-nitrobenzoyl chloride (12.25 g, 66 mmol) was added and mixture was refluxed for 4 hr at 115° C. Reaction was cooled to ambient temperature, poured into ice/water (500 ml), and resulting precipitate was collected by filtration. Precipitate was resuspended in CH2Cl2, left at -20° C for 2 hr, and collected by filtration to yield 18 g (96.7%) of a white powder. LCMS (RT=1.69): 310.1 (100%), 311.2 (15%), 312.1 (3%).

4-amino-N-[3-(trifluoromethyl)phenyl]benzamide (JM7)

4-nitro-N-[3-(trifluoromethyl)phenyl]benzamide (1.55 g, 5 mmol) was dissolved in THF

(50 ml) containing powdered Zn (30 eq). Glacial acetic acid (20 eq) was added and reaction was stirred vigorously overnight under argon gas. Reaction was filtered with celite and solvent was evaporated under reduced pressure. Resulting solid was recrystallized from CH2Cl2 to give 0.78 g (55%) of an orange crystalline solid. LCMS (RT=1.44): 280.1 (100%), 281.1 (10%), 282.1 (3%). NMR, 1H, DMSO (400 MHz): 10.05 (s, 1H), 8.24 (s, 1H), 8.02 (d, 1H), 7.73 (d, 2H), 7.54 (t, 1H), 7.37 (d, 1H), 6.61 (d, 2H), 5.82 (s, 2H).

N-(4-nitrophenyl)-3-(trifluoromethyl)benzamide (JM9)

4-nitroaniline (2.07 g, 15 mmol) and 3-(trifluoromethyl)benzoyl chloride (3.44 g, 16.5 mmol) were used to generate the title compound in a manner similar to JM6 to afford 3.95 g (84.7%) of a yellow crystalline solid. LCMS (RT=2.04): 310.1 (100%), 311.2 (10%), 312.2 (3%).

N-(4-aminophenyl)-3-(trifluoromethyl)benzamide (JM10) was generated in a manner similar to JM7 to afford 0.58 g (41%) of a beige crystalline powder. LCMS (RT=1.03): 280.2 (100%), 281.3 (25%), 282.3 (3%). NMR, 1H, DMSO (400 MHz): 10.10 (s, 1H), 8.25 (s, 1H), 8.23 (d, 1H), 7.92 (d, 1H), 7.75 (t, 1H), 7.37 (d, 2H), 6.55 (d, 2H), 4.97 (s, 2H).

4-({4-[(5-cyclopentyl-1H-pyrazol-3-yl)amino]pyrimidin-2-yl}amino)-N-[3-(trifluoromethyl)phenyl]benzamide (CD12)

JM5 (52.7 mg, 0.2 mmol) and 4-amino-N-[3-(trifluoromethyl)phenyl]benzamide (56.0 mg, 0.2 mmol) were dissolved in n-butanol and heated to 90° C. HCl (30 µl) was added and reaction was stirred under argon gas overnight. Reaction was cooled to ambient temperature, stirbar was removed, and reaction was left at -20° C for 2h. Resulting precipitate was filtered and washed with n-butanol (5 ml) and cold ether (5 ml) to afford a white crystalline powder, which was further purified by HPLC (10-65% ACN/H2O) to afford 26.9 mg (24%) of product. LCMS (RT=1.33): 507.3 (100%), 508.4 (25%), 509.4 (5%). NMR, 1H, DMSO (400 MHz): 9.65 (s, 1H), 9.57 (s, 1H), 8.23 (s, 1H), 8.15 (s, 1H), 8.04-7.98 (m, 2H), 7.91-7.75 (m, 5H), 7.56 (t, 1H), 7.40 (d, 1H), 6.48 (s, 1H), 6.23 (s, 1H), 2.98 (quin, 1H), 2.02-1.93 (m, 2H), 1.73-1.51 (m, 6H).

N-[4-({4-[(5-cyclopentyl-1H-pyrazol-3-yl)amino]pyrimidin-2-yl}amino)phenyl]-3-(trifluoromethyl)benzamide (CD13)

N-(4-aminophenyl)-3-(trifluoromethyl)benzamide (56 mg, 0.20 mmol) and 2-chloro-N-(5-cyclopentyl-1H-pyrazol-3-yl)pyrimidin-4-amine (52.7 mg, 0.20 mmol) were dissolved in n-butanol (3 ml) and heated to 100° C. HCl (33 µl) was added and precipitate observed to form. Reaction was allowed to proceed overnight, cooled to ambient temperature, and precipitate was filtered and washed with cold butanol (5 ml). Product was purified by HPLC (10-75% ACN/H2O) to yield 19.2 mg of a white powder. LCMS (RT=1.42): 507.3 (100%), 508.2 (35%), 509.2 (4%). NMR, 1H, DMSO (400 MHz): 10.37 (s, 1H), 9.58 (s, 1H), 9.12 (s, 1H), 8.29 (s, 1H), 8.26 (d, 1H), 8.14 (s, 1H), 7.98-7.95 (m, 2H), 7.78 (t, 1H), 7.73-7.65 (m, 4H), 6.42 (s, 1H), 6.22 (s, 1H), 2.98 (quin, 1H), 2.05-1.93 (m, 2H), 1.77-1.51 (m, 6H).

4-({4-[(5-cyclopentyl-1H-pyrazol-3-yl)amino]-6-methylpyrimidin-2-yl}amino)-N-[3-(trifluoromethyl)phenyl]benzamide (CD16)

2-chloro-N-(5-cyclopentyl-1H-pyrazol-3-yl)-6-methylpyrimidin-4-amine (83.3 mg, 0.30 mmol) and 4-amino-N-[3-(trifluoromethyl)phenyl]benzamide (84.1 mg, 0.30 mmol) were dissolved in n-butanol (6 ml) and heated to 100° C. HCl was added (50 µl) and reaction allowed to proceed overnight. Mixture was cooled to -20° C for 2h and precipitate was filtered and washed with cold butanol (3 ml) and cold ether (5 ml). Product was purified by HPLC (10-65% ACN/H2O) and 18.1 mg (11%) of a white powder was recovered. LCMS (RT=1.33): 521.3 (100%), 522.4 (28%), 523.3 (4%). NMR, 1H, DMSO (400 MHz): 10.30 (s, 1H), 9.53 (s, 1H), 9.47 (s, 1H), 8.23 (s, 1H), 8.17 (s, 1H), 8.01 (d, 1H), 7.93-7.87 (m, 4H), 7.55 (t, 1H), 7.39 (d, 1H), 6.38 (s, 1H), 6.17 (s, 1H), 2.97 (quin, 1H), 2.20 (s, 3H), 2.01-1.92 (m, 2H), 1.69-1.51 (m, 6H).

N-[4-({4-[(5-cyclopentyl-1H-pyrazol-3-yl)amino]-6-methylpyrimidin-2-yl}amino)phenyl]-3-(trifluoromethyl)benzamide (CD17)

2-chloro-N-(5-cyclopentyl-1H-pyrazol-3-yl)-6-methylpyrimidin-4-amine (41.7 mg, 0.15 mmol) and N-(4-aminophenyl)-3-(trifluoromethyl)benzamide (43 mg, 0.15 mmol) were dissolved in butanol (2 ml), heated to 95° C, and HCl (20 µl) was added. Reaction was allowed to proceed overnight, and cooled to -20° C for 2h. Precipitated was filtered and washed with cold butanol (3 ml) and cold ether (5 ml). Crude solid was purified by HPLC (10-65% ACN/H2O) to give 31.5 mg (40%) of a white solid. LCMS (RT=1.26): 521.3 (100%), 522.4 (28%), 523.4 (4%). NMR, 1H, DMSO (400 MHz): 10.34 (s, 1H), 9.43 (s, 1H), 9.08 (s, 1H), 8.25 (s, 1H), 8.23 (d, 1H), 8.19 (s, 1H), 7.92 (d, 1H), 7.75 (t, 1H), 7.72 (s, 1H), 7.69 (s, 1H), 7.64-7.59 (m, 2H), 6.29 (s, 1H), 6.15 (s, 1H), 2.95 (quin, 1H), 2.17 (s, 3H), 2.00-1.91 (m, 2H), 1.70-1.51 (m, 6H).

CD532 (large scale):

3-(4-aminophenyl)-1-[3-(trifluoromethyl)phenyl]urea (JM149)

P-phenylenediamine (4.33 g, 40 mmol) was dissolved in 100 ml CH2Cl2 in a dried, argon-charged roundbottom flask with stirbar. Mixture was cooled to 0° C before dropwise addition of 3-(trifluoromethyl)phenyl isocyanate (5.64 ml, 40 mmol). Reaction was allowed to warm to ambient temperature over 3 hours, and precipitate was filtered and washed with cold CH2Cl2 (50 ml) to yield a white solid. LCMS (RT=1.10): 295.2 (100%), 296.2 (30%), 297.3 (5%).

1-(4-((4-((5-cyclopentyl-1H-pyrazol-3-yl)amino)pyrimidin-2-yl)amino)phenyl)-3-(3-(trifluoromethyl)phenyl)urea (CD532)

2-chloro-N-(5-cyclopentyl-1H-pyrazol-3-yl)pyrimidin-4-amine (JM5; 1.98 g, 1 mmol) and JM149 (2.21 g, 1 mmol) were dissolved in BuOH 40 ml and stirred at 85° C before dropwise addition of HCl (120 µl). Product formed immediately, and reaction was cooled to ambient temperature and filtered to yield 3.4 g (6.51 mmol, 87%) of a light purple solid. 0.51 g of crude product was purified by HPLC to yield 332 mg of a white solid (65.2% recovery). LCMS (RT=1.32): 522.2 (100%); 523.3 (28%); 524.4 (4%). NMR, 1H, DMSO (400 MHz): 9.69 (s, 1H), 9.51 (s, 1H), 9.29 (s, 1H), 8.94 (s, 1H), 8.25 (s, 1H),

8.04 (s, 1H), 7.91 (d, 1H), 7.65-7.51 (m, 3H), 7.45 (quin, 1H), 7.40-7.32 (m, 2H), 7.23 (d, 1H), 6.32 (s, 1H), 6.19 (s, 1H), 2.93 (quin, 1H), 2.06-1.39 (m, 8H).